Discrete and Continuous Dynamical Systems - Series B
Vol. 31, 2026, pp. 437-465
doi:10.3934/dcdsb.2025116

# A POSITIVITY-PRESERVING SCHEME FOR THE NONLOCAL CAHN-HILLIARD EQUATION WITH LOGARITHMIC POTENTIAL

Yuanyi Sheng[1], Cheng Wang[2] and Zhengru Zhang[*3]

[1]School of Mathematical Sciences, Beijing Normal University, Beijing 100875, China

[2]Department of Mathematics, University of Massachusetts, North Dartmouth, MA 02747, USA

[3]Laboratory of Mathematics and Complex Systems, Beijing Normal University, Beijing 100875, China

(Communicated by Jie Shen)

Abstract. In this paper, we present and analyze a finite difference numerical scheme for the nonlocal Cahn-Hilliard equation with logarithmic Flory-Huggins energy potential. In particular, variable mobility is considered in the gradient flow system for all numerical analyses and tests. To ensure the unique solvability and energy stability, the convex splitting method is applied to the chemical potential, which leads to the implicit treatment for the nonlinear logarithmic terms, the surface diffusion term and the nonlocal term, while the expansive concave term and the mobility are treated explicitly. The positivity preserving property is always preserved at a point-wise level thanks to the singular nature of the logarithmic terms around the values of -1 and 1. In addition, an optimal rate convergence analysis is provided for the proposed numerical scheme. Due to the existence of variable mobility, a higher order asymptotic expansion and the rough error estimate are performed to ensure the uniform bound for numerical solution. Separation property in hand, we finally accomplish the convergence analysis with refined error estimate. Several numerical experiments, especially those designed for nonlocal term, are also presented in this paper, which demonstrate the robustness of the proposed numerical scheme and validate our previous theoretical analysis.

1. **Introduction.** The primary purpose of this paper is to develop an effective numerical scheme for the nonlocal Cahn-Hilliard (NCH) equation with logarithmic Flory-Huggins energy potential. We consider a smooth bounded domain $\Omega \subset \mathbb{R}^d,\ d = 2, 3$. For any $\phi \in H^1(\Omega)$, with a point-wise bound $\phi \in (-1, 1)$, the energy

2020 *Mathematics Subject Classification.* 35K35, 35K55, 49J40, 65M06, 65M12.

*Key words and phrases.* Nonlocal Cahn-Hilliard equation, variable mobility, Flory-Huggins potential, positivity preserving, convex splitting, optimal convergence analysis.

*Corresponding author: Zhengru Zhang.

functional takes the following form

$$\begin{aligned} &E(\phi) = E_1 + E_2, \\ &E_1 = \int_\Omega (1+\phi)\ln(1+\phi) + (1-\phi)\ln(1-\phi) - \frac{\theta_0}{2}\phi^2 + \frac{\varepsilon^2}{2}|\nabla\phi|^2 \mathrm{d}\mathbf{x}, \\ &E_2 = \frac{\sigma}{2}\int_\Omega |(-\Delta)^{-\frac{1}{2}}(\phi - \bar{\phi})|^2 \mathrm{d}\mathbf{x}, \qquad \bar{\phi} = \frac{1}{|\Omega|}\int_\Omega \phi \,\mathrm{d}\mathbf{x}, \end{aligned} \tag{1}$$

where $\theta_0$, $\varepsilon$ and $\sigma$ are positive constants. Parameters $\theta_0$ and $\varepsilon$ are associated with the diffuse interface width [7, 18, 20]. The average $\bar{\phi}$ ($-1 < \bar{\phi} < 1$) stands for the ratio of two homopolymer components. The second part of the energy $E_2$ is the nonlocal item, representing the long-range interactions between copolymers. In fact, the nonlocal item has a more general form [2, 45, 47]

$$E_{nonlocal} = \frac{\sigma}{2}\int_\Omega\int_\Omega G(\mathbf{x}-\mathbf{y})(\phi(\mathbf{x}) - \bar{\phi})(\phi(\mathbf{y}) - \bar{\phi})\,\mathrm{d}\mathbf{y}\,\mathrm{d}\mathbf{x}. \tag{2}$$

The integral form of the nonlocal interactions can be attributed back to van der Waals [49, 53]. If we set $G$ as the Green's function such that $\Delta G(\mathbf{x}-\mathbf{y}) = -\delta(\mathbf{x}-\mathbf{y})$ with periodic boundary condition, where $\delta$ is a Dirac delta function, then (2) becomes $E_2$ in (1). It is clear that when $\sigma = 0$, the energy functional (1) is the common Cahn-Hilliard (CH) energy. With the nonlocal term ($\sigma \neq 0$), $E(\phi)$ is commonly referred to as a Ginzburg-Landau functional with competing or Coulomb-type interactions [43, 51], or the Ohta-Kawasaki (OK) functional first proposed in [48]. In other words, the total free energy (1) for the system is the standard CH free energy supplemented with a nonlocal term.

The evolutional equation to be considered in this paper results from the energetic variation of the energy functional (1) in the $H^{-1}(\Omega)$ Sobolev space. The gradient flow equation becomes

$$\begin{aligned} &\partial_t\phi = \nabla\cdot(\mathcal{M}(\phi)\nabla\mu), \\ &\mu := \partial_\phi E = \ln(1+\phi) - \ln(1-\phi) - \theta_0\phi - \varepsilon^2\Delta\phi + \sigma(-\Delta)^{-1}(\phi - \bar{\phi}), \end{aligned} \tag{3}$$

where $\mathcal{M}(\phi) > 0$ is the mobility function. In most existing studies, the mobility function is typically taken to be constant, meaning the flux of $\phi$ is assumed to be proportional to the force induced by the prescribed chemical potential. However, a more physically accurate assumption in frictional dynamics is that the transfer velocity of $\phi$ is proportional to the force due to the chemical potential [6, 21]. Concentration-dependent mobility appeared in the original derivation of the CH equation [9] and a reasonable choice is [10, 52]

$$\mathcal{M}(\phi) = 1 - \lambda\phi^2 = \lambda(1-\phi)(1+\phi) + (1-\lambda), \quad 0 \le \lambda \le 1. \tag{4}$$

Elliott and Garcke proved the existence of a weak solution to the CH equation with the aforementioned nonconstant mobility for $\lambda = 1$ in [24]. In this case, bulk diffusion vanishes once the phase domains have settled, and the dynamics, which tends to annihilate dissipation and mixing outside the interfacial layer, are then controlled by interfacial diffusion. Zhang and Wang [57] suggested that, at the numerical level, the CH equation with degenerate or near degenerate mobility ($\lambda = 1$ or close to 1 in (4), respectively) provided better numerical resolution and physical fidelity for the multiphase flow simulations of immiscible fluids within the framework of fixed grid computations.

For simplicity of presentation, we consider the periodic boundary condition, while a homogeneous Neumann boundary condition could be similarly treated. As can be

seen in (3), PDE solutions are expected to satisfy a positivity preserving property ($\phi \in (-1,1)$ in a point-wise sense) [24]. Due to the gradient flow structure of (3), the following energy dissipation law holds formally

$$\frac{d}{dt}E(\phi) = -\int_\Omega \mathcal{M}(\phi)|\nabla\mu|^2 \,\mathrm{d}\mathbf{x} \le 0.$$

Meanwhile, the usual mass conservative property is valid, i.e. $\int_\Omega \partial_t\phi \,\mathrm{d}\mathbf{x} = 0$, which follows from the conservative structure of the equation. Thus, a significant numerical issue of the NCH equation is to develop algorithms inheriting energy stable property, mass conservation and positivity preserving property.

As a prototypical gradient flow with respect to a given free energy, the classic CH equation has been successfully used to describe phase separation and coarsening dynamics in binary alloys [8]. Equipped with a nonlocal operator, the NCH equation is capable of capturing more practical phenomena in modeling phase transitions of microstructures compared to the CH equation [26]. Block copolymers are typical examples [32, 33]. In fact, block copolymer melts can self-assemble into specific geometries for manufacturing materials with designed mechanical, optical, and magnetic properties. Apart from materials science, NCH equations have been widely used in many other fields ranging from nanotechnology, image processing to finance. To be specific, in nanotechnology, the model in [56] adds an additional term contributed by the electric field to the equation to guide the diblock copolymer molecules to self-assemble into thin films with layered nanostructures. In the field of image processing, the NCH equation is employed for image inpainting, which involves the restoration of missing or damaged parts of an image based on surrounding data [4, 41]. In financial mathematical models, kernel functions for nonlocal terms arise from expectations over a particular measure used in option pricing [42].

There have been several works on both mathematical and numerical aspects for the NCH models. In the mathematical analysis, [45] provided a mathematical framework of the scaling law for stationary states and the governing equation of morphology. A proof for the instability of n-layered solution of the NCH equation was developed by Ohnishi in [46] with the aid of a spectral comparison theorem between the second and the fourth order NCH equations. Henry et al. discussed the limiting behavior of the solution in [35] as $\varepsilon$ tends to zero. Recently, Gal and Giorgini studied the phase separation property for NCH equations in [27]. Other properties of the NCH equations were investigated by [2, 44, 47], etc.

Due to the complexity of the system (3), especially the inclusion of non-constant mobility and a nonlocal potential, it evidently brings more difficulties in the numerical simulation. Therefore, accurate, stable and efficient numerical schemes are highly desired. Rustum used a hybrid numerical method, which combines exponential time difference (ETD) algorithm and linear iterative gradient stabilization algorithm, to present the global minimizers of NCH equation in [16]. He also analyzed the microphase diagram based upon a density functional theory in [17]. Aristotelous et al. devised a mixed discontinuous Galerkin finite element method in [1], and the temporal discretization was based on a convex splitting of the energy functional. Guan et al. [28, 29, 30] constructed a convex splitting scheme in an alternative way by putting the nonlocal term explicitly. In this way, the nonlocal term can be evaluated only once at each time step. A semi-implicit Fourier spectral method was used in [36] to calculate the minimum energy wavelength of equilibrium

states in diblock copolymers. In [15], an invariant energy quadratization (IEQ) approach was applied to develop a set of second order time-marching schemes for a hydro-dynamically coupled phase field model, in which the free energy contained a long range nonlocal type potential. Du [23] proposed semi-implicit linear numerical methods for solving the NCH equation. The temporal discretization was accomplished by using the stabilization technique, while the spatial discretization was carried out by the Fourier collocation method. A theoretical justification of the energy stability and convergence analysis for these semi-implicit linear schemes has been reported in Li [38, 39, 40], etc. However, most above-mentioned works have been focused on the NCH equation with a constant mobility function and the double-well potential part of the energy is simply treated as a polynomial to avoid the singularities. A preconditioned steepest descent iteration solver is provided in [14], for the variable mobility CH equation. An optimal rate convergence analysis was presented in the paper, while such a discussion was only valid for polynomial-pattern free energy. An optimal rate convergence analysis was presented in the paper, while such a discussion was only valid for polynomial-pattern free energy. As a well known fact, the logarithmic potential energy is considered to be more physically realistic than polynomial free energy, because the former can be derived from regular or ideal solution theories [20]. Chen et al. [12, 13] presented first and second-order accurate temporal algorithms for the variable mobility CH equation with a logarithmic Flory-Huggins energy potential. The positivity-preserving and energy stability analyses were established, whereas the optimal rate convergence estimate was developed only for constant mobility case. If a variable mobility is involved, the coexistence of logarithmic terms and variable mobility requires an $\ell^\infty$ bound for $\phi^{n+1}$ at the next time step to guarantee phase separability. This requirement calls for a higher-order consistency analysis and the application of more advanced technical tools. In this work, we extend the framework of positivity preservation and energy stability to the NCH equation and, more importantly, establish a rigorous convergence analysis for the variable mobility case. It is worth mentioning the key point in the theoretical justification of for positivity-preserving property in [13]; the singular nature of the logarithmic term prevents the numerical solution reaching these singular values as long as the numerical solution stays bounded at the previous time step. This subtle fact also plays a crucial role in the associated analysis.

The standard convex splitting algorithm, pioneered by Eyre's work [25], is a very useful approach to obtain the energy stability at a numerical level. This framework treats the convex part of the chemical potential implicitly and the concave part explicitly. In turn, the energy stability could be theoretically justified by a convexity analysis. Based on this idea, we propose and analyze a convex splitting scheme for NCH equation in this article. The convex-concave decomposition is applied to the energy functional, which in turn leads to an implicit treatment for the nonlinear term, the surface diffusion term and the nonlocal term, combined with an explicit update for the concave term. In addition, an explicit treatment of the mobility function leads to a linear elliptic operator associated with the temporal derivative part. This approach ensures the unique solvability of the numerical scheme, avoids a nonlinear coupling in the numerical implementation, and thereby reduces computational complexity.

The rest of the article is organized as follows. In section 2, the finite difference spatial discretization is reviewed, and some related priori estimates are recalled.

The first order numerical scheme is proposed in Section 3. The unique solvability, positivity preserving property and unconditional energy stability are also proved in this section. In section 4, we conduct the convergence analysis of the numerical scheme with first order temporal accuracy and second order spatial accuracy. Finally, some numerical results are presented in Section 5 and some concluding remarks are given in Section 6.

2. **Finite difference spatial discretization and a few preliminary estimates.** In the spatial discretization, the standard centered finite difference approximation is applied. The computational domain is set as $\Omega = (0, L_x)\times(0, L_y)\times(0, L_z)$. For simplicity, we assume $L_x = L_y = L_z =: L > 0$, and consider a uniform mesh with the grid spacing $h := L/N$ in all directions, where $N \in \mathbb{N}$ is a given number. The case of non-uniform grid could be naturally extended. We first introduce the following two uniform, infinite grids with grid spacing $h > 0$: $E := \{ p_{i+1/2} \,|\, i \in \mathbb{Z} \}$, $C := \{ p_i \,|\, i \in \mathbb{Z} \}$, where $p_i = p(i) := (i-1/2)\cdot h$. The 3D discrete $N^3$-periodic function spaces are defined as follows:

$$\mathcal{C}_{\rm per} := \{ \nu : C \times C \times C \to \mathbb{R} \,|\, \nu_{i,j,k} = \nu_{i+\alpha N, j+\beta N, k+\gamma N},\ \forall i,j,k,\alpha,\beta,\gamma \in \mathbb{Z} \},$$
$$\mathcal{E}^x_{\rm per} := \{ \nu : E \times C \times C \to \mathbb{R} \,|\, \nu_{i+\frac12,j,k} = \nu_{i+\frac12+\alpha N, j+\beta N, k+\gamma N},\ \forall i,j,k,\alpha,\beta,\gamma \in \mathbb{Z} \},$$

with the identification $\nu_{i,j,k} = \nu(p_i, p_j, p_k)$, et cetera. The spaces $\mathcal{E}^y_{\rm per}$ and $\mathcal{E}^z_{\rm per}$ are analogously defined. The functions of $\mathcal{C}_{\rm per}$ are called *cell-centered functions*, and the functions of $\mathcal{E}^x_{\rm per}$, $\mathcal{E}^y_{\rm per}$ and $\mathcal{E}^z_{\rm per}$ are called *face-centered functions*. Hence the center-to-face difference and averaging operators, $A_x$, $D_x : \mathcal{C}_{\rm per} \to \mathcal{E}^x_{\rm per}$, $A_y$, $D_y : \mathcal{C}_{\rm per} \to \mathcal{E}^y_{\rm per}$, and $A_z$, $D_z : \mathcal{C}_{\rm per} \to \mathcal{E}^z_{\rm per}$ can be introduced as

$$A_x\nu_{i+\frac12,j,k} := \frac12(\nu_{i+1,j,k} + \nu_{i,j,k}), \qquad D_x\nu_{i+\frac12,j,k} := \frac1h(\nu_{i+1,j,k} - \nu_{i,j,k}),$$
$$A_y\nu_{i,j+\frac12,k} := \frac12(\nu_{i,j+1,k} + \nu_{i,j,k}), \qquad D_y\nu_{i,j+\frac12,k} := \frac1h(\nu_{i,j+1,k} - \nu_{i,j,k}),$$
$$A_z\nu_{i,j,k+\frac12} := \frac12(\nu_{i,j,k+1} + \nu_{i,j,k}), \qquad D_z\nu_{i,j,k+\frac12} := \frac1h(\nu_{i,j,k+1} - \nu_{i,j,k}).$$

Likewise, we have the face-to-center difference and averaging operators $a_x$, $d_x$ : $\mathcal{E}^x_{\rm per} \to \mathcal{C}_{\rm per}$, $a_y$, $d_y : \mathcal{E}^y_{\rm per} \to \mathcal{C}_{\rm per}$, and $a_z$, $d_z : \mathcal{E}^z_{\rm per} \to \mathcal{C}_{\rm per}$

$$a_x\nu_{i,j,k} := \frac12(\nu_{i+\frac12,j,k} + \nu_{i-\frac12,j,k}), \qquad d_x\nu_{i,j,k} := \frac1h(\nu_{i+\frac12,j,k} - \nu_{i-\frac12,j,k}),$$
$$a_y\nu_{i,j,k} := \frac12(\nu_{i,j+\frac12,k} + \nu_{i,j-\frac12,k}), \qquad d_y\nu_{i,j,k} := \frac1h(\nu_{i,j+\frac12,k} - \nu_{i,j-\frac12,k}),$$
$$a_z\nu_{i,j,k} := \frac12(\nu_{i,j,k+\frac12} + \nu_{i,j,k-\frac12}), \qquad d_z\nu_{i,j,k} := \frac1h(\nu_{i,j,k+\frac12} - \nu_{i,j,k-\frac12}).$$

By introducing $\vec{\mathcal{E}}_{\rm per} := \mathcal{E}^x_{\rm per} \times \mathcal{E}^y_{\rm per} \times \mathcal{E}^z_{\rm per}$, the definitions of the discrete gradient $\nabla_h$ and the discrete divergence $\nabla_h\cdot$ becomes natural:

$$\nabla_h : \mathcal{C}_{\rm per} \to \vec{\mathcal{E}}_{\rm per}, \qquad \nabla_h\nu_{i,j,k} = (D_x\nu_{i+1/2,j,k}, D_y\nu_{i,j+1/2,k}, D_z\nu_{i,j,k+1/2}),$$
$$\nabla_h\cdot : \vec{\mathcal{E}}_{\rm per} \to \mathcal{C}_{\rm per}, \qquad \nabla_h \cdot \vec{f}_{i,j,k} = d_x f^x_{i,j,k} + d_y f^y_{i,j,k} + d_z f^z_{i,j,k},$$

where $\nu \in \mathcal{C}_{\rm per}$, $\vec{f} = (f^x, f^y, f^z) \in \vec{\mathcal{E}}_{\rm per}$. The standard discrete Laplacian $\Delta_h$ : $\mathcal{C}_{\rm per} \to \mathcal{C}_{\rm per}$ in 3D space is given by

$$\begin{aligned}\Delta_h\nu_{i,j,k} &:= \nabla_h \cdot (\nabla_h\nu)_{i,j,k} = d_x(D_x\nu)_{i,j,k} + d_y(D_y\nu)_{i,j,k} + d_z(D_z\nu)_{i,j,k} \\ &= \frac{1}{h^2}(\nu_{i+1,j,k} + \nu_{i-1,j,k} + \nu_{i,j+1,k} + \nu_{i,j-1,k} + \nu_{i,j,k+1} + \nu_{i,j,k-1} - 6\nu_{i,j,k}).\end{aligned}$$

More generally, if $g$ is a periodic scalar function defined at all of the face center points and $\vec{f} \in \vec{\mathcal{E}}_{\rm per}$, then $g\vec{f} \in \vec{\mathcal{E}}_{\rm per}$, by taking point-wise multiplication; we may define

$$\nabla_h \cdot (g\vec{f})_{i,j,k} = d_x(g \cdot f^x)_{i,j,k} + d_y(g \cdot f^y)_{i,j,k} + d_z(g \cdot f^z)_{i,j,k}.$$

Specifically, if $\nu \in \mathcal{C}_{\rm per}$, then $\nabla_h \cdot (g\nabla_h) : \mathcal{C}_{\rm per} \to \mathcal{C}_{\rm per}$ is defined point-wise via

$$\nabla_h \cdot (g\nabla_h \nu)_{i,j,k} = d_x(g \cdot D_x\nu)_{i,j,k} + d_y(g \cdot D_y\nu)_{i,j,k} + d_z(g \cdot D_z\nu)_{i,j,k}.$$

Now we are ready to introduce the grid inner products for $\mathcal{C}_{\rm per}$, $\mathcal{E}^x_{\rm per}$ and $\vec{\mathcal{E}}_{\rm per}$, respectively.

$$\langle \nu, \xi \rangle_\Omega := h^3 \sum_{i,j,k=1}^{N} \nu_{i,j,k}\xi_{i,j,k}, \quad \nu,\, \xi \in \mathcal{C}_{\rm per}, \qquad [\nu, \xi]_{\rm x} := \langle a_x(\nu\xi), 1\rangle_\Omega,\ \nu,\, \xi \in \mathcal{E}^x_{\rm per},$$

$$[\vec{f}_1, \vec{f}_2]_\Omega := [f_1^x, f_2^x]_{\rm x} + [f_1^y, f_2^y]_{\rm y} + [f_1^z, f_2^z]_{\rm z}, \qquad \vec{f}_i = (f_i^x, f_i^y, f_i^z) \in \vec{\mathcal{E}}_{\rm per},\ i = 1, 2.$$

Meanwhile, $[\nu, \xi]_{\rm y}$, $[\nu, \xi]_{\rm z}$ in $\mathcal{E}^y_{\rm per}$ and $\mathcal{E}^z_{\rm per}$ can be analogously formulated. In turn, we construct the following norms for grid functions: $\|\nu\|_2^2 := \langle \nu, \nu\rangle_\Omega$, for $\nu \in \mathcal{C}_{\rm per}$; $\|\nu\|_p^p := \langle |\nu|^p, 1\rangle_\Omega$, for $1 \le p < \infty$, and $\|\nu\|_\infty := \max_{1\le i,j,k\le N} |\nu_{i,j,k}|$. Norms of the discrete gradient are defined as follows:

$$\|\nabla_h \nu\|_2^2 := [\nabla_h\nu, \nabla_h\nu]_\Omega = [D_x\nu, D_x\nu]_{\rm x} + [D_y\nu, D_y\nu]_{\rm y} + [D_z\nu, D_z\nu]_{\rm z}, \quad \forall \nu \in \mathcal{C}_{\rm per},$$
$$\|\nabla_h \nu\|_p^p := [|D_x\nu|^p, 1]_{\rm x} + [|D_y\nu|^p, 1]_{\rm y} + [|D_z\nu|^p, 1]_{\rm z}, \quad \forall \nu \in \mathcal{C}_{\rm per}, \quad 1 \le p < \infty.$$

In addition, higher order norms can be defined. For example,

$$\|\nu\|_{H_h^1}^2 := \|\nu\|_2^2 + \|\nabla_h\nu\|_2^2, \qquad \|\nu\|_{H_h^2}^2 := \|\nu\|_{H_h^1}^2 + \|\Delta_h\nu\|_2^2, \qquad \forall \nu \in \mathcal{C}_{\rm per}.$$

**Lemma 2.1** ([55]). *Let $g$ be an arbitrary periodic, scalar function defined on all of the face center points. For any $\psi,\, \nu \in \mathcal{C}_{\rm per}$ and any $\vec{f} \in \vec{\mathcal{E}}_{\rm per}$, the following summation by parts are valid:*

$$\langle \psi, \nabla_h \cdot \vec{f}\,\rangle_\Omega = -\left[\nabla_h\psi, \vec{f}\,\right]_\Omega, \quad \langle \psi, \nabla_h \cdot (g\nabla_h\nu)\rangle_\Omega = -[\nabla_h\psi, g\nabla_h\nu]_\Omega.$$

To facilitate the convergence analysis, a discrete analogue of the $H^{-1}_{\rm per}(\Omega)$ space [54] is required. Firstly, the mean zero space is defined as

$$\mathring{\mathcal{C}}_{\rm per} := \left\{ \psi \in \mathcal{C}_{\rm per} \,\middle|\, 0 = \bar{\psi} := \frac{h^3}{|\Omega|} \sum_{i,j,k=1}^{N} \psi_{i,j,k} \right\}.$$

For any $\phi \in \mathcal{C}_{\rm per}$ with $\bar{\phi} := |\Omega|^{-1}\langle \phi, 1\rangle_\Omega$, we can immediately obtain $\phi - \bar{\phi} \in \mathring{\mathcal{C}}_{\rm per}$. The $H^{-1}_{\rm per}(\Omega)$ space is a subset of $\mathring{\mathcal{C}}_{\rm per}$ that satisfies the following conditions. For any $\phi \in \mathcal{C}_{\rm per}$, there exists a unique $\psi \in \mathring{\mathcal{C}}_{\rm per}$ that solves

$$\mathcal{L}_{\mathcal{D}}(\psi) := -\nabla_h \cdot (\mathcal{D}\nabla_h\psi) = \phi - \bar{\phi}.$$

In this equation, $\mathcal{D}$ is a positive, periodic scalar function defined at all of the face center points. We then define a bilinear form

$$\langle \phi_1, \phi_2 \rangle_{\mathcal{L}_{\mathcal{D}}^{-1}} := [\mathcal{D}\nabla_h\psi_1, \nabla_h\psi_2]_\Omega, \quad \phi_1,\, \phi_2 \in \mathring{\mathcal{C}}_{\rm per},$$

where $\psi_i \in \mathring{\mathcal{C}}_{\rm per}$ is the unique solution to

$$\mathcal{L}_{\mathcal{D}}(\psi_i) := -\nabla_h \cdot (\mathcal{D}\nabla_h\psi_i) = \phi_i, \quad i = 1,\, 2.$$

**Lemma 2.2** ([54]). *$\langle\cdot,\cdot\rangle_{\mathcal{L}_{\mathcal{D}}^{-1}}$ is an inner product and has the following identity*

$$\langle\phi_1,\phi_2\rangle_{\mathcal{L}_{\mathcal{D}}^{-1}} = \big\langle\phi_1,\mathcal{L}_{\mathcal{D}}^{-1}(\phi_2)\big\rangle_\Omega = \big\langle\mathcal{L}_{\mathcal{D}}^{-1}(\phi_1),\phi_2\big\rangle_\Omega, \quad \phi_1,\ \phi_2\in\mathring{\mathcal{C}}_{\rm per}.$$

*We denote the norm associated to this inner product as*

$$\|\phi\|_{\mathcal{L}_{\mathcal{D}}^{-1}} := \sqrt{\langle\phi,\phi\rangle_{\mathcal{L}_{\mathcal{D}}^{-1}}}, \quad \forall\phi\in\mathring{\mathcal{C}}_{\rm per}.$$

**Remark 2.3.** When $\mathcal{D}\equiv 1$, the subscripts are simplified to $\langle\cdot,\cdot\rangle_{\mathcal{L}_{\mathcal{D}}^{-1}} =: \langle\cdot,\cdot\rangle_{-1,h}$, $\|\cdot\|_{\mathcal{L}_{\mathcal{D}}^{-1}} =: \|\cdot\|_{-1,h}$. In turn, we have

$$\langle f,g\rangle_{-1,h} := \langle f,(-\Delta_h)^{-1}g\rangle_\Omega = \langle(-\Delta_h)^{-1}f,g\rangle_\Omega, \qquad \|f\|_{-1,h} := \sqrt{\langle f,f\rangle_{-1,h}}.$$

The following discrete Sobolev inequalities for grid functions have been derived in previous works, which play significant roles in our proof of convergence analysis.

**Lemma 2.4** ([14][22][54]). *For any 3-D periodic grid function $f$ (over cell centered mesh points), we have the following discrete Sobolev inequalities*

$$\|f\|_4\le C\|f\|_{H_h^1}, \quad \|f\|_\infty\le C(\|f\|_2+\|\Delta_h f\|_2),$$
$$\|\nabla_h f\|_4\le C\|\Delta_h f\|_2, \quad \|\nabla_h f\|_4\le C\|\nabla_h f\|_2^{\frac14}\cdot\|\Delta_h f\|_2^{\frac34},$$

*in which the positive constant $C$ only depends on the domain $\Omega$.*

3. **A first order numerical scheme.** In this section, we construct and analyze a first order accurate (in time) numerical scheme for solving the NCH equation (3). The finite difference approximations defined in last section are used for spatial discretization. We follow the convex-concave decomposition methodology and the first order scheme is constructed as follows: given $\phi^n\in\mathcal{C}_{\rm per}$, find $\phi^{n+1},\ \mu^{n+1}\in\mathcal{C}_{\rm per}$ such that

$$\frac{\phi^{n+1}-\phi^n}{\Delta t} = \nabla_h\cdot(\check{\mathcal{M}}^n\nabla_h\mu^{n+1}), \tag{5}$$

where

$$\mu^{n+1} := \ln(1+\phi^{n+1})-\ln(1-\phi^{n+1})-\theta_0\phi^n-\varepsilon^2\Delta_h\phi^{n+1}+\sigma(-\Delta_h)^{-1}(\phi^{n+1}-\overline{\phi^{n+1}}).$$

The discrete mobility $\check{\mathcal{M}}^n$ is evaluated at the face center points

$$\check{\mathcal{M}}^n_{i+1/2,j,k} = A_x(\mathcal{M}(\phi^n))_{i+1/2,j,k}, \qquad \check{\mathcal{M}}^n_{i,j+1/2,k} = A_y(\mathcal{M}(\phi^n))_{i,j+1/2,k},$$
$$\check{\mathcal{M}}^n_{i,j,k+1/2} = A_z(\mathcal{M}(\phi^n))_{i,j,k+1/2}.$$

If the solution exists, it is obvious that the numerical scheme is mass-conservative, i.e. $\overline{\phi^{n+1}}=\overline{\phi^n}=\cdots=\overline{\phi^0}=:\beta_0$, since

$$\big\langle\phi^{n+1}-\phi^n,1\big\rangle_\Omega = \Delta t\,\big\langle\nabla_h\cdot(\check{\mathcal{M}}^n\nabla_h\mu^{n+1}),1\big\rangle_\Omega = -\Delta t\,\big[\check{\mathcal{M}}^n\nabla_h\mu^{n+1},\nabla_h 1\big]_\Omega = 0.$$

Naturally, a point-wise bound for the grid function $\phi^{n+1}$, specifically $-1<\phi^{n+1}_{i,j,k}<1$, must be preserved to ensure that the numerical scheme is well-defined. This property will be established in the subsequent theorem. Prior to that, it is necessary to introduce an operator and a norm related to discrete mobility.

**Definition 3.1.** For any $\phi\in\mathring{\mathcal{C}}_{\rm per}$, there exists a unique $\psi\in\mathring{\mathcal{C}}_{\rm per}$ that solves

$$\mathcal{L}_{\check{\mathcal{M}}^n}(\psi) := -\nabla_h\cdot(\check{\mathcal{M}}^n\nabla_h\psi) = \phi.$$

In turn, the corresponding norm may be introduced:

$$\|\phi\|_{\mathcal{L}^{-1}_{\check{\mathcal{M}}^n}} = \sqrt{\langle\phi,\mathcal{L}^{-1}_{\check{\mathcal{M}}^n}(\phi)\rangle_\Omega}.$$

**Lemma 3.2** ([13]). *Assume that for all $x \in [-1,1]$, $\mathcal{M}(x) \geq \mathcal{M}_0 > 0$. Suppose that $\phi_1,\ \phi_2 \in \mathcal{C}_{\rm per}$, with $\phi_1 - \phi_2 \in \mathring{\mathcal{C}}_{\rm per}$, and that $\|\phi_1\|_\infty < 1$, and $\|\phi_2\|_\infty \leq M_1$. Then, we have the following estimate:*

$$\|\mathcal{L}^{-1}_{\breve{\mathcal{M}}^n}(\phi_1 - \phi_2)\|_\infty \leq C,$$

*where $C > 0$ depends only on $M_1$, $\mathcal{M}_0$, $h$ and $\Omega$. In particular, if $\mathcal{M}(\phi) \equiv 1$, then $C$ is independent of the mesh spacing $h$.*

### 3.1. **Positivity-preserving property and unique solvability.**

**Theorem 3.3.** *Assume that for all $x \in [-1,1]$, $\mathcal{M}(x) \geq \mathcal{M}_0 > 0$. Given $\phi^n \in \mathcal{C}_{\rm per}$ with $\|\phi^n\|_\infty \leq M_1$ for some $M_1 > 0$, and $|\overline{\phi^n}| < 1$, there exists a unique solution $\phi^{n+1} \in \mathcal{C}_{\rm per}$ to (5), such that $\phi^{n+1} - \overline{\phi^n} \in \mathring{\mathcal{C}}_{\rm per}$ and $\|\phi^{n+1}\|_\infty < 1$.*

*Proof.* If a valid numerical solution exists, it must satisfy the mass conservation identity, namely $\phi^{n+1} - \overline{\phi^n} \in \mathring{\mathcal{C}}_{\rm per}$. Set $\beta_0 := \overline{\phi^n}$. The numerical solution of (5) is a minimizer of the following strictly convex discrete energy functional

$$\begin{aligned}\mathcal{J}^n(\phi) := \frac{1}{2\Delta t}\|\phi - \phi^n\|^2_{\mathcal{L}^{-1}_{\breve{\mathcal{M}}^n}} + \langle 1+\phi, \ln(1+\phi)\rangle_\Omega + \langle 1-\phi, \ln(1-\phi)\rangle_\Omega \\ + \frac{\varepsilon^2}{2}\|\nabla_h\phi\|_2^2 - \theta_0\langle \phi, \phi^n\rangle_\Omega + \frac{\sigma}{2}\|\phi - \bar{\phi}\|^2_{-1,h},\end{aligned} \tag{6}$$

over the admissible set

$$A_h := \{\phi \in \mathcal{C}_{\rm per} |\ \|\phi\|_\infty \leq 1,\ \langle \phi - \beta_0, 1\rangle_\Omega = 0\} \subset \mathbb{R}^{N^3}.$$

We further let $\varphi = \phi - \beta_0$ and transform the energy functional (6) into

$$\begin{aligned}\mathcal{F}^n(\varphi) &:= \mathcal{J}^n(\varphi + \beta_0) \\ &= \frac{1}{2\Delta t}\|\varphi + \beta_0 - \phi^n\|^2_{\mathcal{L}^{-1}_{\breve{\mathcal{M}}^n}} + \frac{\sigma}{2}\|\varphi\|^2_{-1,h} + \langle 1+\varphi+\beta_0, \ln(1+\varphi+\beta_0)\rangle_\Omega \\ &\quad + \langle 1-\varphi-\beta_0, \ln(1-\varphi-\beta_0)\rangle_\Omega + \frac{\varepsilon^2}{2}\|\nabla_h\varphi\|_2^2 - \theta_0\langle \varphi+\beta_0, \phi^n\rangle_\Omega,\end{aligned}$$

defined on the corresponding set

$$\mathring{A}_h := \left\{\varphi \in \mathring{\mathcal{C}}_{\rm per} | -1-\beta_0 \leq \varphi \leq 1-\beta_0\right\} \subset \mathbb{R}^{N^3}.$$

If $\varphi \in \mathring{A}_h$ minimizes $\mathcal{F}^n$, then $\phi = \varphi + \beta_0 \in A_h$ minimizes $\mathcal{J}^n$, and vice versa.

We now prove the existence of a minimizer for $\mathcal{F}^n$ over the domain $\mathring{A}_h$. Considering the following closed domain:

$$\mathring{A}_{h,\delta} := \left\{\varphi \in \mathring{\mathcal{C}}_{\rm per} |\ \delta - 1 - \beta_0 \leq \varphi \leq 1 - \delta - \beta_0\right\} \subset \mathbb{R}^{N^3},$$

where $\delta \in (0, 1/2)$ is sufficiently small. Since $\mathring{A}_{h,\delta}$ is a bounded, compact, and convex subset of $\mathring{\mathcal{C}}_{\rm per}$, there exists a (not necessarily unique) minimizer of $\mathcal{F}^n$ over $\mathring{A}_{h,\delta}$. The central aspect of the positivity-preserving analysis is that such a minimizer cannot occur on the boundary of $\mathring{A}_{h,\delta}$, provided $\delta$ is sufficiently small. In fact, the boundary of $\mathring{A}_{h,\delta}$ is defined as the set of points $\psi \in \mathring{A}_{h,\delta}$ for which $\|\psi+\beta_0\|_\infty = 1-\delta$.

To derive a contradiction, suppose $\varphi^\star$ is the minimizer of $\mathcal{F}^n$ and occurs at a boundary point of $\mathring{A}_{h,\delta}$. Then there exists at least one grid point $\vec{\alpha}_0 = (i_0, j_0, k_0)$ such that $|\varphi^\star_{\vec{\alpha}_0} + \beta_0| = 1-\delta$. Without loss of generality, it is assumed that $\varphi^\star_{\vec{\alpha}_0} + \beta_0 = \delta - 1$. In this case, the grid function $\varphi^\star$ has a global minimum at $\vec{\alpha}_0$. Assume that

$\vec{\alpha}_1 = (i_1, j_1, k_1)$ is a grid point where $\varphi^\star$ attains its maximum. By the fact that $\overline{\varphi^\star} = 0$, it is obvious that $\varphi^\star_{\vec{\alpha}_1} \geq 0$ and

$$1 - \delta \geq \varphi^\star_{\vec{\alpha}_1} + \beta_0 \geq \beta_0. \tag{7}$$

Since $\mathcal{F}^n$ is smooth over $\mathring{A}_{h,\delta}$, the directional derivative for all $\psi \in \mathring{\mathcal{C}}_{\text{per}}$ turns out to be

$$\begin{aligned} &d_s\mathcal{F}^n(\varphi^\star + s\psi)|_{s=0} \\ &= \frac{1}{\Delta t}\langle \mathcal{L}^{-1}_{\check{\mathcal{M}}^n}(\varphi^\star - \phi^n + \beta_0), \psi\rangle_\Omega + \langle \ln(1+\varphi^\star+\beta_0) - \ln(1-\varphi^\star-\beta_0), \psi\rangle_\Omega \\ &\quad - \langle \theta_0\phi^n + \varepsilon^2\Delta_h\varphi^\star, \psi\rangle_\Omega + \sigma\langle(-\Delta_h)^{-1}\varphi^\star, \psi\rangle_\Omega. \end{aligned} \tag{8}$$

If we pick the particular direction $\psi \in \mathring{\mathcal{C}}_{\text{per}}$ as

$$\psi_{i,j,k} = \delta_{i,i_0}\delta_{j,j_0}\delta_{k,k_0} - \delta_{i,i_1}\delta_{j,j_1}\delta_{k,k_1},$$

where $\delta_{i,j}$ is the Dirac delta function, the derivative can be expressed as

$$\begin{aligned} &\frac{1}{h^3} d_s\mathcal{F}^n(\varphi^\star + s\psi)|_{s=0} \\ &= \ln(1+\varphi^\star_{\vec{\alpha}_0}+\beta_0) - \ln(1-\varphi^\star_{\vec{\alpha}_0}-\beta_0) - \ln(1+\varphi^\star_{\vec{\alpha}_1}+\beta_0) + \ln(1-\varphi^\star_{\vec{\alpha}_1}-\beta_0) \\ &\quad - \theta_0(\phi^n_{\vec{\alpha}_0} - \phi^n_{\vec{\alpha}_1}) - \varepsilon^2(\Delta_h\varphi^\star_{\vec{\alpha}_0} - \Delta_h\varphi^\star_{\vec{\alpha}_1}) + \sigma(-\Delta_h)^{-1}\varphi^\star_{\vec{\alpha}_0} - \sigma(-\Delta_h)^{-1}\varphi^\star_{\vec{\alpha}_1} \\ &\quad + \frac{1}{\Delta t}\mathcal{L}^{-1}_{\check{\mathcal{M}}^n}(\varphi^\star - \phi^n + \beta_0)_{\vec{\alpha}_0} - \frac{1}{\Delta t}\mathcal{L}^{-1}_{\check{\mathcal{M}}^n}(\varphi^\star - \phi^n + \beta_0)_{\vec{\alpha}_1}. \end{aligned}$$

To simplify the expression, a rewritten form $\phi^\star := \varphi^\star + \beta_0$ gives

$$\begin{aligned} \frac{1}{h^3} d_s\mathcal{F}^n(\varphi^\star + s\psi)|_{s=0} = \ln(1+\phi^\star_{\vec{\alpha}_0}) - \ln(1-\phi^\star_{\vec{\alpha}_0}) - \ln(1+\phi^\star_{\vec{\alpha}_1}) + \ln(1-\phi^\star_{\vec{\alpha}_1}) \\ - \theta_0(\phi^n_{\vec{\alpha}_0} - \phi^n_{\vec{\alpha}_1}) - \varepsilon^2(\Delta_h\phi^\star_{\vec{\alpha}_0} - \Delta_h\phi^\star_{\vec{\alpha}_1}) \\ + \frac{1}{\Delta t}\mathcal{L}^{-1}_{\check{\mathcal{M}}^n}(\phi^\star - \phi^n)_{\vec{\alpha}_0} - \frac{1}{\Delta t}\mathcal{L}^{-1}_{\check{\mathcal{M}}^n}(\phi^\star - \phi^n)_{\vec{\alpha}_1} \\ + \sigma(-\Delta_h)^{-1}(\phi^\star - \beta_0)_{\vec{\alpha}_0} - \sigma(-\Delta_h)^{-1}(\phi^\star - \beta_0)_{\vec{\alpha}_1}. \end{aligned} \tag{9}$$

By the fact that $\phi^\star_{\vec{\alpha}_0} = -1 + \delta$ and (7), it follows that

$$\ln(1+\phi^\star_{\vec{\alpha}_0}) - \ln(1-\phi^\star_{\vec{\alpha}_0}) - \ln(1+\phi^\star_{\vec{\alpha}_1}) + \ln(1-\phi^\star_{\vec{\alpha}_1}) \leq \ln\frac{\delta}{2-\delta} - \ln\frac{1+\beta_0}{1-\beta_0}. \tag{10}$$

A-priori assumption $\|\phi^n\|_\infty \leq M_1$ at the previous time step indicates an estimate

$$-2M_1 \leq \phi^n_{\vec{\alpha}_0} - \phi^n_{\vec{\alpha}_1} \leq 2M_1. \tag{11}$$

Since $\phi^\star$ takes a minimum at the grid point $\vec{\alpha}_0$ and a maximum at the grid point $\vec{\alpha}_1$, we see that

$$\Delta_h\phi^\star_{\vec{\alpha}_0} \geq 0, \qquad \Delta_h\phi^\star_{\vec{\alpha}_1} \leq 0. \tag{12}$$

For the last four terms appearing in (9), an application of Lemma 3.2 reveals that

$$-2C_1 \leq \mathcal{L}^{-1}_{\check{\mathcal{M}}^n}(\phi^\star - \phi^n)_{\vec{\alpha}_0} - \mathcal{L}^{-1}_{\check{\mathcal{M}}^n}(\phi^\star - \phi^n)_{\vec{\alpha}_1} \leq 2C_1, \tag{13}$$

$$-2C_2 \leq (-\Delta_h)^{-1}(\phi^\star - \beta_0)_{\vec{\alpha}_0} - (-\Delta_h)^{-1}(\phi^\star - \beta_0)_{\vec{\alpha}_1} \leq 2C_2. \tag{14}$$

Consequently, a substitution of (10) through (14) into (9) yields the following bound on the directional derivative:

$$\frac{1}{h^3} d_s\mathcal{F}^n(\varphi^\star + s\psi)|_{s=0} \leq \ln\frac{\delta}{2-\delta} - \ln\frac{1+\beta_0}{1-\beta_0} + C_3, \quad C_3 := 2M_1\theta_0 + 2C_1\Delta t^{-1} + 2C_2\sigma.$$

Notice that as $\Delta t \to 0$, $C_3$ becomes singular. Meanwhile, $C_3$ is a constant for any fixed $\Delta t$, which allows us to choose $\delta \in (0, 1/2)$ sufficiently small such that

$$\frac{1}{h^3} d_s \mathcal{F}^n(\varphi^\star + s\psi)|_{s=0} \le \ln \frac{\delta}{2-\delta} - \ln \frac{1+\beta_0}{1-\beta_0} + C_3 < 0.$$

This contradicts the earlier assumption that $\mathcal{F}^n$ attains a minimum at $\varphi^\star$, as the directional derivative is negative in a direction pointing into the interior of $\mathring{A}_{h,\delta}$.

Similarly, we are also able to prove that the global minimum of $\mathcal{F}^n$ over $\mathring{A}_{h,\delta}$ cannot occur at a boundary point $\varphi^\star$ where $\varphi^\star_{\vec{\alpha}_0} + \beta_0 = 1 - \delta$, for some $\vec{\alpha}_0$. These combined two facts imply that the global minimum of $\mathcal{F}^n$ over $\mathring{A}_{h,\delta}$ can only occur at an interior point $\varphi \in (\mathring{A}_{h,\delta})^o \subset (\mathring{A}_h)^o$. Consequently, there exists a solution $\phi = \varphi + \beta_0 \in A_h$ that minimizes $\mathcal{J}^n$ over $A_h$, which corresponds to the numerical solution of (5). Hence, the existence of the numerical solution is established.

In addition, the uniqueness of this numerical solution is straightforward, since $\mathcal{J}^n$ is a strictly convex function over $A_h$. This completes the proof. □

3.2. **Unconditional energy stability.** Now we analyze the energy stability of the proposed scheme (5). The discrete energy $E_h(\phi) : \mathcal{C}_{\text{per}} \to \mathbb{R}$ is defined as

$$E_h(\phi) = \langle 1+\phi, \ln(1+\phi)\rangle_\Omega + \langle 1-\phi, \ln(1-\phi)\rangle_\Omega - \frac{\theta_0}{2}\|\phi\|_2^2 + \frac{\varepsilon^2}{2}\|\nabla_h \phi\|_2^2 + \frac{\sigma}{2}\|\phi - \bar{\phi}\|_{-1,h}^2.$$

Because of the convex-concave decomposition structure of the numerical scheme, an unconditional energy stability is available. The subordinate theorem articulates this property.

**Theorem 3.4.** *Assume that for all $x \in [-1, 1]$, $\mathcal{M}(x) \ge \mathcal{M}_0 > 0$. The numerical scheme (5) is unconditionally energy stable for any time step $\Delta t > 0$, grid spacing $h > 0$ in the sense that*

$$E_h(\phi^{n+1}) \le E_h(\phi^n), \quad \forall n \in \mathbb{N}. \tag{15}$$

*By recursion, we obtain $E_h(\phi^{n+1}) \le E_h(\phi^0) \le C_4$, where $C_4 > 0$ is independent of $h$.*

*Proof.* Taking an inner product with (5) by $\Delta t \mu^{n+1}$ yields

$$\langle \phi^{n+1} - \phi^n, \mu^{n+1}\rangle_\Omega = \Delta t \langle \nabla_h \cdot (\check{\mathcal{M}}^n \nabla_h \mu^{n+1}), \mu^{n+1}\rangle_\Omega \le -\mathcal{M}_0 \Delta t \|\nabla_h \mu^{n+1}\|_2^2 \le 0.$$

On the other hand, we observe the following expansion:

$$\begin{aligned} &\langle \phi^{n+1} - \phi^n, \mu^{n+1}\rangle_\Omega \\ &= \langle \phi^{n+1} - \phi^n, \ln(1+\phi^{n+1}) - \ln(1-\phi^{n+1})\rangle_\Omega - \theta_0 \langle \phi^{n+1} - \phi^n, \phi^n\rangle_\Omega \\ &\quad - \varepsilon^2 \langle \phi^{n+1} - \phi^n, \Delta_h \phi^{n+1}\rangle_\Omega + \sigma \langle \phi^{n+1} - \phi^n, (-\Delta_h)^{-1}(\phi^{n+1} - \overline{\phi^{n+1}})\rangle_\Omega. \end{aligned} \tag{16}$$

By the convexity of the logarithmic terms $\langle 1+\phi, \ln(1+\phi)\rangle$, $\langle 1-\phi, \ln(1-\phi)\rangle$, the following estimate is valid

$$\begin{aligned} &\langle \phi^{n+1} - \phi^n, \ln(1+\phi^{n+1}) - \ln(1-\phi^{n+1})\rangle_\Omega \\ &\ge \langle 1+\phi^{n+1}, \ln(1+\phi^{n+1})\rangle_\Omega + \langle 1-\phi^{n+1}, \ln(1-\phi^{n+1})\rangle_\Omega \\ &\quad - \langle 1+\phi^n, \ln(1+\phi^n)\rangle_\Omega - \langle 1-\phi^n, \ln(1-\phi^n)\rangle_\Omega. \end{aligned} \tag{17}$$

An application of the identity $\mathbf{a} \cdot (\mathbf{a} - \mathbf{b}) = \frac{1}{2}|\mathbf{a}|^2 - \frac{1}{2}|\mathbf{b}|^2 + \frac{1}{2}|\mathbf{a} - \mathbf{b}|^2$ indicates that

$$-\langle \phi^{n+1} - \phi^n, \theta_0 \phi^n\rangle_\Omega \ge -\frac{\theta_0}{2}(\|\phi^{n+1}\|_2^2 - \|\phi^n\|_2^2), \tag{18}$$

$$-\varepsilon^2\langle\phi^{n+1}-\phi^n,\Delta_h\phi^{n+1}\rangle_\Omega\geq\frac{\varepsilon^2}{2}(\|\nabla_h\phi^{n+1}\|_2^2-\|\nabla_h\phi^n\|_2^2). \tag{19}$$

For the nonlocal item, by the fact that $\phi^{n+1}-\overline{\phi^{n+1}}\in\mathring{\mathcal{C}}_{\rm per}$, combined with the mass conservation identity, i.e. $\overline{\phi^{n+1}}=\overline{\phi^n}$, we see that

$$\begin{aligned}
&\langle\phi^{n+1}-\phi^n,(-\Delta_h)^{-1}(\phi^{n+1}-\overline{\phi^{n+1}})\rangle_\Omega\\
=&\langle\phi^{n+1}-\phi^n,(-\Delta_h)^{-1}(\phi^{n+1}-\overline{\phi^{n+1}})\rangle_\Omega-(\overline{\phi^{n+1}}-\overline{\phi^n})\langle 1,(-\Delta_h)^{-1}(\phi^{n+1}-\overline{\phi^{n+1}})\rangle_\Omega\\
=&\langle\phi^{n+1}-\phi^n,(-\Delta_h)^{-1}(\phi^{n+1}-\overline{\phi^{n+1}})\rangle_\Omega-\langle\overline{\phi^{n+1}}-\overline{\phi^n},(-\Delta_h)^{-1}(\phi^{n+1}-\overline{\phi^{n+1}})\rangle_\Omega\\
=&\langle(\phi^{n+1}-\overline{\phi^{n+1}})-(\phi^n-\overline{\phi^n}),(-\Delta_h)^{-1}(\phi^{n+1}-\overline{\phi^{n+1}})\rangle_\Omega\\
=&\frac{1}{2}\left(\|\phi^{n+1}-\overline{\phi^{n+1}}\|_{-1,h}^2-\|\phi^n-\overline{\phi^n}\|_{-1,h}^2+\|(\phi^{n+1}-\overline{\phi^{n+1}})-(\phi^n-\overline{\phi^n})\|_{-1,h}^2\right)\\
\geq&\frac{1}{2}\|\phi^{n+1}-\overline{\phi^{n+1}}\|_{-1,h}^2-\frac{1}{2}\|\phi^n-\overline{\phi^n}\|_{-1,h}^2.
\end{aligned} \tag{20}$$

A substitution of (17) - (20) into (16) leads to (15), so that the unconditional energy stability is proved. □

**Remark 3.5.** Due to the energy dissipation, we have

$$\|\nabla_h\phi^{n+1}\|_2^2\leq 2\varepsilon^{-2}(E_h(\phi^{n+1})+\frac{\theta_0}{2}|\Omega|)\leq\varepsilon^{-2}(2C_4+\theta_0|\Omega|).$$

As a result, the discrete $H_h^1$ estimate $\|\nabla_h\phi^{n+1}\|_2\leq\varepsilon^{-1}\sqrt{2C_4+\theta_0|\Omega|}=:C_5$, for any $n\in\mathbb{N}$, is established.

4. **Optimal rate convergence analysis.** Now we proceed into the convergence analysis. Denote by $\Phi$ the exact PDE solution to the NCH system (3). With sufficiently regular initial data, it is reasonable to assume that $\Phi$ has regularity of class $\mathcal{R}$:

$$\Phi\in\mathcal{R}:=H^4(0,T;C_{\rm per}(\Omega))\cap H^3(0,T;C_{\rm per}^2(\Omega))\cap L^\infty(0,T;C_{\rm per}^8(\Omega)).$$

Moreover, the following separation property is valid for the exact solution:

$$1+\Phi\geq\varepsilon_0,\quad 1-\Phi\geq\varepsilon_0,\quad\text{for some }\varepsilon_0>0\text{ at a point-wise level.} \tag{21}$$

Define the Fourier projection of the exact solution as $\Phi_N(\cdot,t):=\mathcal{P}_N\Phi(\cdot,t)$, a projection into $\mathfrak{B}^K$, the space of trigonometric polynomials of degree up to and including $K$ (with $N=2K+1$). Subsequently, the projection approximation is standard: if $\Phi\in L^\infty(0,T;H_{\rm per}^l(\Omega))$, for any $l\in\mathbb{N}$,

$$\|\Phi_N-\Phi\|_{L^\infty(0,T;H^k)}\leq Ch^{l-k}\|\Phi\|_{L^\infty(0,T;H^l)},\quad 0\leq k\leq l. \tag{22}$$

The Fourier projection does not inherently preserve the positivity of $1+\Phi_N$ and $1-\Phi_N$. However, we are able to enforce the phase separation property by taking $h$ sufficiently small to ensure that $1+\Phi_N\geq\frac{3}{4}\varepsilon_0$ and $1-\Phi_N\geq\frac{3}{4}\varepsilon_0$.

We denote $\Phi_N^n=\Phi_N(\cdot,t_n)$ with $t_n=n\Delta t$, and $\phi_N^n:=\mathcal{P}_h\Phi_N(\cdot,t_n)$ as the values of $\Phi_N$ at discrete grid points at time $t_n$, specifically $(\phi_N^n)_{i,j,k}=\Phi_N(x_i,y_j,z_k,t=t_n)$. The mass conservation identity is available at the discrete level:

$$\int_\Omega\Phi_N(\cdot,t_n)\,{\rm d}\mathbf{x}=\int_\Omega\Phi(\cdot,t_n)\,{\rm d}\mathbf{x}=\int_\Omega\Phi(\cdot,t_{n-1})\,{\rm d}\mathbf{x}=\int_\Omega\Phi_N(\cdot,t_{n-1})\,{\rm d}\mathbf{x},\ \forall n\in\mathbb{N}_+, \tag{23}$$

in which the first and third steps are based on the fact that $\Phi_N$ is the Fourier projection of $\Phi$ and the second step is based on the fact that the exact solution $\Phi$ is mass conservative at the continuous level. On the other hand, the numerical solution (5) is also mass conservative at the discrete level:

$$\overline{\phi^{n+1}} = \overline{\phi^n}, \quad \forall\, n \in \mathbb{N}.$$

Since $\Phi_N \in \mathfrak{B}^K$, it always holds that

$$\int_\Omega \Phi_N(\cdot, t_n)\, \mathrm{d}\mathbf{x} = h^2 \sum_{i,j,k} \Phi_N(x_i, y_j, z_k, t_n) = h^2 \sum_{i,j,k} (\phi_N^n)_{i,j,k}.$$

Therefore, the mass conservative property $\overline{\phi_N^n} = \overline{\phi_N^{n-1}}$ is available at the discrete level. We choose the initial data as $\phi^0 = \phi_N^0 = \mathcal{P}_h \Phi_N(\cdot, t = 0)$, and define the error grid function

$$e_\phi^n := \phi_N^n - \phi^n, \quad \forall n \in \mathbb{N}.$$

It follows that $\overline{e_\phi^n} = 0$. Therefore, the discrete norm $\|\cdot\|_{-1,h}$ is well defined for the error grid function $e_\phi^n$.

The following theorem is the main result of this section.

**Theorem 4.1.** *Assume that for all $x \in [-1, 1]$, the inequality $0 < \mathcal{M}_0 \le \mathcal{M}(x) \le \mathcal{M}_1 < \infty$ and $|\mathcal{M}'(x)| \le M$ holds, where $M$ is a constant. Given initial data $\Phi(\cdot, t = 0) \in \mathcal{C}^6_{\mathrm{per}}(\Omega)$, and suppose the exact solution for NCH equation (3) is of regularity class $\mathcal{R}$. Then, provided $\Delta t$ and $h$ are sufficiently small, under the linear refinement requirement $C_1 h \le \Delta t \le C_2 h$ we have*

$$\|e_\phi^n\|_2 + \Big(\Delta t \sum_{m=1}^{n} \|\Delta_h e_\phi^m\|_2^2\Big)^{1/2} \le C(\Delta t + h^2), \tag{24}$$

*for all positive integers $n$, such that $t_n = n\Delta t \le T$. In (24), $C > 0$ is independent of $n$, $\Delta t$ and $h$.*

4.1. **Higher order consistency analysis.** By consistency, the projection solution $\Phi_N$ solves the discrete equation (5) with first-order accuracy in time and second-order accuracy in space. However, this leading local truncation error is insufficient to recover an a-priori $\ell^\infty$ bound of the numerical solution. To remedy this, we have to develop a higher order consistency analysis by constructing a supplementary field $\Phi_{\Delta t}$ and defining the following profile

$$\hat{\Phi} = \Phi_N + \Delta t \mathcal{P}_N \Phi_{\Delta t}.$$

Notice that $\Phi_{\Delta t}$ is a continuous function derived from a perturbation expansion and depends solely on the exact solution $\Phi$; its construction will be outlined later. In other words, a higher-order approximate expansion of the exact solution is introduced. Instead of a direct comparison between the numerical and exact solutions, we estimate the numerical error function between the constructed profile and the numerical solution. This approach of higher-order consistency enables us to derive a higher-order convergence estimate, which in turn leads to the desired $\|\cdot\|_\infty$ bound of the numerical solution through an application of inverse inequality.

We begin with the truncation error analysis for the temporal discretization by using a straightforward Taylor expansion in time, as well as estimate (22) for the projection solution:

$$\frac{\Phi_N^{n+1} - \Phi_N^n}{\Delta t} = \nabla \cdot \big(\mathcal{M}(\Phi_N^n) \nabla \mu_N^{n+1}\big) + \Delta t (G^{(0)})^n + O(\Delta t^2) + O(h^{m_0}), \tag{25}$$

$$\mu_N^{n+1} = \ln(1+\Phi_N^{n+1}) - \ln(1-\Phi_N^{n+1}) - \theta_0\Phi_N^n - \varepsilon^2\Delta\Phi_N^{n+1} + \sigma(-\Delta)^{-1}(\Phi_N^{n+1} - \overline{\Phi_N^{n+1}}). \tag{26}$$

Here $m_0 \geq 4$ and the function $G^{(0)}$, which depends only on the higher-order derivatives of $\Phi_N$, is smooth enough in the sense that its derivatives are bounded. Meanwhile, because of the mass conservation identity

$$\int_\Omega (\Phi_N^{n+1} - \Phi_N^n)\,\mathrm{d}\mathbf{x} = 0, \quad \int_\Omega \nabla\cdot\left(\mathcal{M}(\Phi_N^n)\nabla\mu_N^{n+1}\right)\,\mathrm{d}\mathbf{x} = 0,$$

we can obtain

$$\int_\Omega (G^{(0)})^n\,\mathrm{d}\mathbf{x} = 0. \tag{27}$$

In turn, the correction function $\Phi_{\Delta t}$ is given by solving the following equation:

$$\partial_t\Phi_{\Delta t} = \nabla\cdot(\mathcal{M}(\Phi_N)\nabla\mathcal{V}_{\Delta t} + \mathcal{M}'(\Phi_N)\Phi_{\Delta t}\nabla\mu_N) - G^{(0)}, \tag{28}$$

$$\mathcal{V}_{\Delta t} = \frac{\Phi_{\Delta t}}{1+\Phi_N} + \frac{\Phi_{\Delta t}}{1-\Phi_N} - \theta_0\Phi_{\Delta t} - \varepsilon^2\Delta\Phi_{\Delta t} + \sigma(-\Delta)^{-1}\Phi_{\Delta t}, \tag{29}$$

$$\mu_N = \ln(1+\Phi_N) - \ln(1-\Phi_N) - \theta_0\Phi_N - \varepsilon^2\Delta\Phi_N + \sigma(-\Delta)^{-1}(\Phi_N - \overline{\Phi_N}), \tag{30}$$

with the periodic boundary condition. The existence of a solution to the above linear PDE system is straightforward. Since the correction function depends solely on the projection solution $\Phi_N$, which preserves sufficient regularity, the derivatives of $\Phi_{\Delta t}$ in various orders are bounded. Also, trivial initial data $\Phi_{\Delta t}(\cdot, t=0) \equiv 0$ could be imposed to equation (28). In combination with the identity (27), we get

$$\int_\Omega \partial_t\Phi_{\Delta t}\,\mathrm{d}\mathbf{x} = \int_\Omega \nabla\cdot(\mathcal{M}(\Phi_N)\nabla\mathcal{V}_{\Delta t} + \mathcal{M}'(\Phi_N)\Phi_{\Delta t}\nabla\mu_N)\,\mathrm{d}\mathbf{x} - \int_\Omega G^{(0)}\,\mathrm{d}\mathbf{x} = 0,$$

so that the mass conservative property is valid:

$$\int_\Omega \Phi_{\Delta t}(\cdot,t)\,\mathrm{d}\mathbf{x} = \int_\Omega \Phi_{\Delta t}(\cdot,t=0)\,\mathrm{d}\mathbf{x} = 0, \quad \forall t > 0. \tag{31}$$

An application of semi-implicit discretization (as given by (25)) to (28) - (30) implies that

$$\frac{\Phi_{\Delta t}^{n+1} - \Phi_{\Delta t}^n}{\Delta t} = \nabla\cdot\left(\mathcal{M}(\Phi_N^n)\nabla\mathcal{V}_{\Delta t}^{n+1} + \mathcal{M}'(\Phi_N^n)\Phi_{\Delta t}^n\nabla\mu_N^{n+1}\right) - (G^{(0)})^n + O(\Delta t), \tag{32}$$

$$\mathcal{V}_{\Delta t}^{n+1} = \frac{\Phi_{\Delta t}^{n+1}}{1+\Phi_N^{n+1}} + \frac{\Phi_{\Delta t}^{n+1}}{1-\Phi_N^{n+1}} - \theta_0\Phi_{\Delta t}^n - \varepsilon^2\Delta\Phi_{\Delta t}^{n+1} + \sigma(-\Delta)^{-1}\Phi_{\Delta t}^{n+1}, \tag{33}$$

$$\mu_N^{n+1} = \ln(1+\Phi_N^{n+1}) - \ln(1-\Phi_N^{n+1}) - \theta_0\Phi_N^n - \varepsilon^2\Delta\Phi_N^{n+1} + \sigma(-\Delta)^{-1}(\Phi_N^{n+1} - \overline{\Phi_N^{n+1}}). \tag{34}$$

Therefore, a combination of (25) - (26) and a Fourier projection of (32) - (34) leads to the desired second order consistency estimate of $\hat{\Phi} = \Phi_N + \Delta t\mathcal{P}_N\Phi_{\Delta t}$ in time:

$$\frac{\hat{\Phi}^{n+1} - \hat{\Phi}^n}{\Delta t} = \nabla\cdot\left(\mathcal{M}(\hat{\Phi}^n)\nabla\hat{\mu}^{n+1}\right) + O(\Delta t^2) + O(h^{m_0}), \tag{35}$$

$$\hat{\mu}^{n+1} = \ln(1+\hat{\Phi}^{n+1}) - \ln(1-\hat{\Phi}^{n+1}) - \theta_0\hat{\Phi}^n - \varepsilon^2\Delta\hat{\Phi}^{n+1} + \sigma(-\Delta)^{-1}(\hat{\Phi}^{n+1} - \overline{\hat{\Phi}^{n+1}}), \tag{36}$$

in which the following linearized expansions have been utilized

$$\ln(1\pm\hat{\Phi}) = \ln(1\pm\Phi_N \pm \Delta t\mathcal{P}_N\Phi_{\Delta t}) = \ln(1\pm\Phi_N) \pm \frac{\Delta t\mathcal{P}_N\Phi_{\Delta t}}{1\pm\Phi_N} + O(\Delta t^2).$$

Because of the mass conservative property for $\Phi_{\Delta t}$, as derived in (31), the subsequent identities are natural

$$\int_\Omega \mathcal{P}_N \Phi_{\Delta t}(\cdot,t)\,\mathrm{d}\mathbf{x} = 0, \quad \forall t>0, \tag{37}$$

$$\int_\Omega \hat{\Phi}(\cdot,t)\,\mathrm{d}\mathbf{x} = \int_\Omega \Phi_N(\cdot,t)\,\mathrm{d}\mathbf{x}, \quad \forall t>0. \tag{38}$$

As a result, we see that

$$\begin{aligned} \frac{1}{|\Omega|}\int_\Omega \hat{\Phi}^{n+1}\,\mathrm{d}\mathbf{x} &= \frac{1}{|\Omega|}\int_\Omega \hat{\Phi}^{n}\,\mathrm{d}\mathbf{x} = \cdots = \frac{1}{|\Omega|}\int_\Omega \hat{\Phi}^{0}\,\mathrm{d}\mathbf{x} \\ &= \frac{1}{|\Omega|}\int_\Omega \Phi_N(\cdot,t=0)\,\mathrm{d}\mathbf{x} = \overline{\phi^0} = \overline{\phi^n} = \overline{\phi^{n+1}}, \quad \forall n\in\mathbb{N}. \end{aligned} \tag{39}$$

Finally, an application of finite difference approximation, combined with the Taylor expansion in space, yields a truncation error estimate for the constructed solution

$$\frac{\hat{\Phi}^{n+1}-\hat{\Phi}^n}{\Delta t} = \nabla_h\cdot\left(\check{\mathcal{M}}(\hat{\Phi}^n)\nabla_h\hat{\mu}^{n+1}\right)+\tau^{n+1}, \tag{40}$$

$$\hat{\mu}^{n+1} = \ln(1+\hat{\Phi}^{n+1})-\ln(1-\hat{\Phi}^{n+1})-\theta_0\hat{\Phi}^n-\varepsilon^2\Delta_h\hat{\Phi}^{n+1}+\sigma(-\Delta_h)^{-1}(\hat{\Phi}^{n+1}-\overline{\hat{\Phi}^{n+1}}), \tag{41}$$

where

$$\|\tau^{n+1}\|_{-1,h}\le C(\Delta t^2+h^2).$$

It is noticed that $\tau^{n+1}$ has a zero mean, $\overline{\tau^{n+1}}=0$, at the discrete level for any $n\in\mathbb{N}$, based on the estimate (39) and the fact that $\hat{\Phi}^n\in\mathfrak{B}^K$.

**Remark 4.2.** The term $\Phi_{\Delta t}$ does not have a specific physical meaning; its construction is based on the idea of perturbation analysis of the numerical scheme in terms of the time step size. The contribution of $\Phi_{\Delta t}$ to improving the accuracy of the error estimate relies on the Taylor expansion of the exact solution and the asymptotic analysis in terms of $\Delta t$. In turn, the constructed profile $\hat{\Phi}=\Phi_N+\Delta t\mathcal{P}_N\Phi_{\Delta t}$ satisfies the numerical scheme with a higher order consistency. Mathematically, $\Phi_{\Delta t}$ is related to the projected exact solution $\Phi_N$ through equations (28) - (30), and is used to cancel the leading truncation error term $G^{(0)}$ in (25). The purpose of such a higher-order asymptotic expansion and truncation error estimate is to maintain a sufficiently high order accuracy to apply inverse inequalities, ultimately deriving the a-priori $\ell^\infty$ bound for the numerical solution to obtain the separation property. With this property for both the constructed approximate solution and the numerical solution, the nonlinear error term can be appropriately analyzed in the $\ell^\infty(0,T;H_h^1)$ convergence estimate.

**Remark 4.3.** Since the correction function $\Phi_{\Delta t}$ depends solely on the exact solution $\Phi$ and is therefore bounded, the separation property (21) for $\Phi$ can similarly hold for $\hat{\Phi}$

$$1+\hat{\Phi}\ge\varepsilon_0^\star, \quad 1-\hat{\Phi}\ge\varepsilon_0^\star, \quad for\ \varepsilon_0^\star=\frac{\varepsilon_0}{2}>0, \tag{42}$$

provided that $\Delta t$ and $h$ are sufficiently small, in which the projection estimate (22) has been repeatedly used. Moreover, its discrete $W_h^{1,\infty}$ norm will remain bounded

$$\|\hat{\Phi}^k\|_\infty\le C^\star, \quad \|\nabla_h\hat{\Phi}^k\|_\infty\le C^\star, \quad \forall k\ge 0.$$

These uniform bounds will be used in the following convergence analysis.

4.2. **Rough error estimate.** Instead of a direct analysis for the error function $e_\phi^n$, we estimate the error between the numerical solution and the constructed solution to obtain a higher order convergence. In turn, the following perturbed numerical error function is introduced:

$$\tilde{\phi}^n := \mathcal{P}_h \hat{\Phi}^n - \phi^n, \quad \forall n \in \mathbb{N}.$$

The fact that $\hat{\Phi}^n \in \mathfrak{B}^K$ and equation (39) result in the discrete zero-mean property of the numerical error function $\overline{\tilde{\phi}^n} = 0$. Consequently, the discrete $\|\cdot\|_{-1,h}$ norm of this error function is well-defined.

Subtracting the numerical scheme (5) from (40) - (41) gives

$$\frac{\tilde{\phi}^{n+1} - \tilde{\phi}^n}{\Delta t} = \nabla_h \cdot \left( \check{\mathcal{M}}(\phi^n) \nabla_h \tilde{\mu}^{n+1} + \left( \check{\mathcal{M}}(\hat{\Phi}^n) - \check{\mathcal{M}}(\phi^n) \right) \nabla_h \hat{\mu}^{n+1} \right) + \tau^{n+1}, \quad (43)$$

with the following expansions

$$\begin{aligned}
\tilde{\mu}^{n+1} =& \ln(1+\hat{\Phi}^{n+1}) - \ln(1+\phi^{n+1}) - \ln(1-\hat{\Phi}^{n+1}) + \ln(1-\phi^{n+1}) \\
& - \theta_0 \tilde{\phi}^n - \varepsilon^2 \Delta_h \tilde{\phi}^{n+1} + \sigma(-\Delta_h)^{-1} \tilde{\phi}^{n+1}, \\
\hat{\mu}^{n+1} =& \ln(1+\hat{\Phi}^{n+1}) - \ln(1-\hat{\Phi}^{n+1}) - \theta_0 \hat{\Phi}^n - \varepsilon^2 \Delta_h \hat{\Phi}^{n+1} \\
& + \sigma(-\Delta_h)^{-1} (\hat{\Phi}^{n+1} - \overline{\hat{\Phi}^{n+1}}).
\end{aligned}$$

Since $\hat{\mu}^{n+1}$ only depends on the exact solution and the constructed profiles, it is reasonable to assume a discrete $W_h^{1,\infty}$ bound

$$\|\hat{\mu}^{n+1}\|_{W_h^{1,\infty}} \le C^\star. \quad (44)$$

In addition, we make the following assumptions for the previous time step

$$\|\tilde{\phi}^n\|_2 \le \Delta t^{\frac{15}{8}} + h^{\frac{15}{8}}, \quad \|\Delta_h \tilde{\phi}^n\|_2 \le \Delta t^{\frac{11}{8}} + h^{\frac{11}{8}}. \quad (45)$$

These a-priori assumptions will be recovered through the convergence analysis at the next time step, as will be demonstrated later. As a consequence of these a-priori assumptions, the discrete $\ell^\infty$ and $W_h^{1,4}$ bounds could be derived, based on the discrete Sobolev inequality (see Lemma 2.4) and the linear refinement requirement $C_1 h \le \Delta t \le C_2 h$

$$\begin{aligned}
&\|\tilde{\phi}^n\|_\infty \le C(\|\tilde{\phi}^n\|_2 + \|\Delta_h \tilde{\phi}^n\|_2) \le C(\Delta t^{\frac{11}{8}} + h^{\frac{11}{8}}) \le \frac{\varepsilon_0^\star}{2} \le 1, \quad (46) \\
&\|\nabla_h \tilde{\phi}^n\|_4 \le \|\Delta_h \tilde{\phi}^n\|_2 \le \Delta t^{\frac{11}{8}} + h^{\frac{11}{8}} \le 1.
\end{aligned}$$

Subsequently, the following estimate is available for the numerical solution at the previous time step

$$\|\phi^n\|_\infty \le \|\hat{\Phi}^n\|_\infty + \|\tilde{\phi}^n\|_\infty \le C^\star + 1 =: \tilde{C}_3, \quad (47)$$

$$\|\nabla_h \phi^n\|_4 \le \|\nabla_h \hat{\Phi}^n\|_4 + \|\nabla_h \tilde{\phi}^n\|_4 \le \tilde{C}_3. \quad (48)$$

A combination of the $\ell^\infty$ estimate (46) for the error function and the separation estimate (42) leads to a similar separation property for the numerical solution at the previous time step, in a point-wise sense

$$\frac{\varepsilon_0^\star}{2} \le 1 + \phi^n \le 2, \quad \frac{\varepsilon_0^\star}{2} \le 1 - \phi^n \le 2.$$

The following lemma states the result of a rough error estimate.

**Lemma 4.4.** *Under the regularity requirement assumption (44) and the a-priori assumptions (45), a rough error estimate is valid for the numerical error evolutionary system (43)*

$$\|\tilde{\phi}^{n+1}\|_2 + \|\nabla_h \tilde{\phi}^{n+1}\|_2 \le C(\Delta t^{\frac{5}{4}} + h^{\frac{5}{4}}). \tag{49}$$

*Proof.* Taking a discrete inner product with (43) by $\tilde{\mu}^{n+1}$ leads to

$$\begin{aligned} &\frac{1}{\Delta t}\langle \tilde{\phi}^{n+1}, \tilde{\mu}^{n+1}\rangle + \langle \check{\mathcal{M}}(\phi^n)\nabla_h \tilde{\mu}^{n+1}, \nabla_h \tilde{\mu}^{n+1}\rangle \\ &\quad = \frac{1}{\Delta t}\langle \tilde{\phi}^{n}, \tilde{\mu}^{n+1}\rangle - \langle (\check{\mathcal{M}}(\hat{\Phi}^n) - \check{\mathcal{M}}(\phi^n))\nabla_h \hat{\mu}^{n+1}, \nabla_h \tilde{\mu}^{n+1}\rangle + \langle \tau^{n+1}, \tilde{\mu}^{n+1}\rangle, \end{aligned} \tag{50}$$

in which summation by parts formulas have been repeatedly applied. Since $\mathcal{M}(\phi)$ is bounded below, it is clear that

$$\langle \check{\mathcal{M}}(\phi^n)\nabla_h \tilde{\mu}^{n+1}, \nabla_h \tilde{\mu}^{n+1}\rangle \ge \mathcal{M}_0 \|\nabla_h \tilde{\mu}^{n+1}\|_2^2.$$

Leveraging the mean-free property of the truncation error $\tau$, we obtain the following estimate

$$\langle \tau^{n+1}, \tilde{\mu}^{n+1}\rangle \le \|\tau^{n+1}\|_{-1,h} \cdot \|\nabla_h \tilde{\mu}^{n+1}\|_2 \le \frac{1}{\mathcal{M}_0}\|\tau^{n+1}\|_{-1,h}^2 + \frac{\mathcal{M}_0}{4}\|\nabla_h \tilde{\mu}^{n+1}\|_2^2.$$

A similar bound is valid for the $\langle \tilde{\phi}^n, \tilde{\mu}^{n+1}\rangle$ term:

$$\langle \tilde{\phi}^n, \tilde{\mu}^{n+1}\rangle \le \|\tilde{\phi}^n\|_{-1,h} \cdot \|\nabla_h \tilde{\mu}^{n+1}\|_2 \le \frac{1}{\mathcal{M}_0 \Delta t}\|\tilde{\phi}^n\|_{-1,h}^2 + \frac{\mathcal{M}_0 \Delta t}{4}\|\nabla_h \tilde{\mu}^{n+1}\|_2^2.$$

For the second term on the right-hand side of (50), it is observed that

$$\begin{aligned} &- \langle (\check{\mathcal{M}}(\hat{\Phi}^n) - \check{\mathcal{M}}(\phi^n))\nabla_h \hat{\mu}^{n+1}, \nabla_h \tilde{\mu}^{n+1}\rangle \\ &\le \|\nabla_h \hat{\mu}^{n+1}\|_\infty \cdot \|\check{\mathcal{M}}(\hat{\Phi}^n) - \check{\mathcal{M}}(\phi^n)\|_2 \cdot \|\nabla_h \tilde{\mu}^{n+1}\|_2 \\ &\le C^\star M \|\tilde{\phi}^n\|_2 \cdot \|\nabla_h \tilde{\mu}^{n+1}\|_2 \le \frac{(C^\star)^2 M^2}{\mathcal{M}_0}\|\tilde{\phi}^n\|_2^2 + \frac{\mathcal{M}_0}{4}\|\nabla_h \tilde{\mu}^{n+1}\|_2^2. \end{aligned} \tag{51}$$

The second inequality comes from the fact that the derivation of mobility function is bounded, i.e. $|\mathcal{M}'(\phi)| \le M$. Hence the following estimate is valid

$$|\check{\mathcal{M}}(\hat{\Phi}^n) - \check{\mathcal{M}}(\phi^n)| = |\mathcal{M}'(\xi^{(n)})(\hat{\Phi}^n - \phi^n)| = |\mathcal{M}'(\xi^{(n)})\tilde{\phi}^n| \le M|\tilde{\phi}^n|,$$

where $\xi^{(n)}$ takes a value between $\phi^n$ and $\hat{\Phi}^n$. Notice that a uniform bound for the mobility function, and the $W_h^{1,\infty}$ bound for $\hat{\mu}^{n+1}$, have been used in the derivation.

For the last term on the left-hand side of (50), an application of the mean value theorem yields a point-wise representation

$$\ln(1+\hat{\Phi}^{n+1}) - \ln(1+\phi^{n+1}) = \frac{\tilde{\phi}^{n+1}}{1+\eta^{(n+1)}}, \quad \eta^{(n+1)} \text{ is between } \phi^{n+1} \text{ and } \hat{\Phi}^{n+1}.$$

By the point-wise bound $-1 < \phi^{n+1},\ \hat{\Phi}^{n+1} < 1$, we conclude that $0 < 1+\eta^{(n+1)} < 2$, and hence

$$\langle \tilde{\phi}^{n+1}, \ln(1+\hat{\Phi}^{n+1}) - \ln(1+\phi^{n+1})\rangle = \langle \tilde{\phi}^{n+1}, \frac{\tilde{\phi}^{n+1}}{1+\eta^{(n+1)}}\rangle \ge \frac{1}{2}\|\tilde{\phi}^{n+1}\|_2^2.$$

A similar analysis becomes available

$$-\langle \tilde{\phi}^{n+1}, \ln(1-\hat{\Phi}^{n+1}) - \ln(1-\phi^{n+1})\rangle \ge \frac{1}{2}\|\tilde{\phi}^{n+1}\|_2^2.$$

The last three terms in the expansion of $\langle \tilde{\phi}^{n+1}, \tilde{\mu}^{n+1} \rangle$ will be analyzed in a straightforward manner

$$
\begin{aligned}
&-\theta_0 \langle \tilde{\phi}^{n+1}, \tilde{\phi}^n \rangle \geq -\frac{1}{2}\theta_0^2 \|\tilde{\phi}^n\|_2^2 - \frac{1}{2}\|\tilde{\phi}^{n+1}\|_2^2, \\
&-\langle \tilde{\phi}^{n+1}, \Delta_h \tilde{\phi}^{n+1} \rangle = \|\nabla_h \tilde{\phi}^{n+1}\|_2^2, \\
&\langle \tilde{\phi}^{n+1}, (-\Delta_h)^{-1} \tilde{\phi}^{n+1} \rangle = \|\tilde{\phi}^{n+1}\|_{-1,h}^2 \geq 0.
\end{aligned}
$$

Then we arrive at

$$
\langle \tilde{\phi}^{n+1}, \tilde{\mu}^{n+1} \rangle \geq \frac{1}{2}\|\tilde{\phi}^{n+1}\|_2^2 - \frac{1}{2}\theta_0^2 \|\tilde{\phi}^n\|_2^2 + \varepsilon^2 \|\nabla_h \tilde{\phi}^{n+1}\|_2^2.
$$

A combination of the above estimates gives

$$
\begin{aligned}
&\frac{1}{2}\|\tilde{\phi}^{n+1}\|_2^2 + \varepsilon^2 \|\nabla_h \tilde{\phi}^{n+1}\|_2^2 + \frac{\mathcal{M}_0 \Delta t}{4}\|\nabla_h \tilde{\mu}^{n+1}\|_2^2 \\
&\leq \left( \frac{\theta_0^2}{2} + \frac{(C^\star)^2 M^2 \Delta t}{\mathcal{M}_0} \right) \|\tilde{\phi}^n\|_2^2 + \frac{1}{\mathcal{M}_0 \Delta t}\|\tilde{\phi}^n\|_{-1,h}^2 + \frac{\Delta t}{\mathcal{M}_0}\|\tau^{n+1}\|_{-1,h}^2.
\end{aligned} \tag{52}
$$

For the right-hand side of inequality (52), the following estimates are available:

$$
\begin{aligned}
&\frac{1}{\mathcal{M}_0 \Delta t}\|\tilde{\phi}^n\|_{-1,h}^2 \leq \frac{C}{\mathcal{M}_0 \Delta t}\|\tilde{\phi}^n\|_2^2 \leq C(\Delta t^{\frac{11}{4}} + h^{\frac{11}{4}}), \\
&\frac{\theta_0^2}{2}\|\tilde{\phi}^n\|_2^2 \leq C(\Delta t^{\frac{15}{4}} + h^{\frac{15}{4}}), \\
&\frac{(C^\star)^2 M^2 \Delta t}{\mathcal{M}_0}\|\tilde{\phi}^n\|_2^2 \leq C(\Delta t^{\frac{19}{4}} + h^{\frac{19}{4}}), \\
&\frac{\Delta t}{\mathcal{M}_0}\|\tau^{n+1}\|_{-1,h}^2 \leq C\Delta t \|\tau^{n+1}\|_2^2 \leq C(\Delta t^5 + h^5).
\end{aligned}
$$

These estimates are derived from the a-priori assumptions, the fact that $\|f\|_{-1,h} \leq C\|f\|_2$, as well as the refinement constraint $C_1 h \leq \Delta t \leq C_2 h$. Consequently we obtain

$$
\|\tilde{\phi}^{n+1}\|_2 + \|\nabla_h \tilde{\phi}^{n+1}\|_2 \leq C(\Delta t^{\frac{11}{8}} + h^{\frac{11}{8}}) \leq \hat{C}(\Delta t^{\frac{5}{4}} + h^{\frac{5}{4}}), \tag{53}
$$

provided that $\Delta t$ and $h$ are sufficiently small. In (53), $\hat{C}$ is independent of the time step $\Delta t$ and the spatial step $h$. The proof of the rough error estimate is complete. □

The rough error estimate (49) reveals that

$$
\|\tilde{\phi}^{n+1}\|_\infty \leq \frac{C\|\tilde{\phi}^{n+1}\|_{H_h^1}}{h^{\frac{1}{2}}} \leq \hat{C}_1(\Delta t^{\frac{3}{4}} + h^{\frac{3}{4}}) \leq \frac{\varepsilon_0^\star}{2}, \tag{54}
$$

$$
\|\tilde{\phi}^{n+1}\|_4 \leq C\|\tilde{\phi}^{n+1}\|_{H_h^1} \leq C(\Delta t^{\frac{5}{4}} + h^{\frac{5}{4}}), \tag{55}
$$

provided $\Delta t$ and $h$ are sufficiently small. In the derivation, the linear refinement requirement $C_1 h \leq \Delta t \leq C_2 h$, along with the 3D inverse inequality and the discrete Sobolev inequality (Lemma 2.4), have been utilized. Furthermore, a combination of (54) and the separation property (42) leads to the following separation property of the numerical solution at the next time step $t^{n+1}$:

$$
\frac{\varepsilon_0^\star}{2} \leq 1 + \phi^{n+1} \leq 2, \quad \frac{\varepsilon_0^\star}{2} \leq 1 - \phi^{n+1} \leq 2. \tag{56}
$$

Such a uniform bound will play a crucial role in the refined error estimate.

**Remark 4.5.** It is observed that the accuracy order in (49) is at least half an order higher than the $\ell^\infty$ error rate in (54), which comes from an application of the inverse inequality. To ensure a sufficient order for the $\ell^\infty$ estimate of $\phi^{n+1}$, and thereby maintain the separation property at the next time step, we make the a-priori assumption (45) at the previous time step. By the above discussion, it is clear that the fractional exponents in (45) are not unique.

4.3. **Refined error estimate.** We begin this subsection by stating the following preliminary results necessary for the refined error analysis.

**Lemma 4.6** ([31]). *Based on the separation property (56) for numerical solution and the discrete $\|\cdot\|_4$ rough estimation (55), we have*

$$\|\nabla_h \mathcal{L}^{n+1}\|_2 \le 4(\varepsilon_0^\star)^{-1}\|\nabla_h \tilde\phi^{n+1}\|_2 + C(\varepsilon_0^\star)^{-2}\|\tilde\phi^{n+1}\|_4 + \theta_0\|\nabla_h\tilde\phi^n\|_2,$$

*where*

$$\mathcal{L}^{n+1} = \ln(1+\hat\Phi^{n+1}) - \ln(1+\phi^{n+1}) - \ln(1-\hat\Phi^{n+1}) + \ln(1-\phi^{n+1}) - \theta_0\tilde\phi^n.$$

**Lemma 4.7.** *For any $k \ge 0$, define $\tilde\psi^k = (-\Delta_h)^{-1}\tilde\phi^k$. The estimate is valid:*

$$\|\nabla_h\tilde\psi^k\|_2 \le \tilde C_4\|\tilde\phi^k\|_2,$$

*for some constant $\tilde C_4 > 0$ that is independent of $h$.*

*Proof.* It is a direct consequence of the standard estimate $\|f\|_{-1,h} \le C\|f\|_2$, for any $f$ satisfies $\overline{f} = 0$. □

Now we proceed into the refined error estimate. Taking a discrete inner product with (43) by $2\tilde\phi^{n+1}$ leads to

$$\begin{aligned}\frac{1}{\Delta t}\left(\|\tilde\phi^{n+1}\|_2^2 - \|\tilde\phi^n\|_2^2 + \|\tilde\phi^{n+1}-\tilde\phi^n\|_2^2\right) + 2\langle\check{\mathcal{M}}(\phi^n)\nabla_h\tilde\mu^{n+1}, \nabla_h\tilde\phi^{n+1}\rangle \\ = -2\langle(\check{\mathcal{M}}(\hat\Phi^n) - \check{\mathcal{M}}(\phi^n))\nabla_h\hat\mu^{n+1}, \nabla_h\tilde\phi^{n+1}\rangle + 2\langle\tau^{n+1}, \tilde\phi^{n+1}\rangle,\end{aligned} \tag{57}$$

where summation-by-parts formulas have been applied. The local truncation error term can be analyzed using the Cauchy inequality

$$2\langle\tau^{n+1}, \tilde\phi^{n+1}\rangle \le \|\tau^{n+1}\|_2^2 + \|\tilde\phi^{n+1}\|_2^2. \tag{58}$$

For the second term on the left-hand-side of (57), we begin with a rewritten form:

$$\begin{aligned}\langle\check{\mathcal{M}}(\phi^n)\nabla_h\tilde\mu^{n+1}, \nabla_h\tilde\phi^{n+1}\rangle &= \langle\check{\mathcal{M}}(\phi^n)\nabla_h\mathcal{L}^{n+1}, \nabla_h\tilde\phi^{n+1}\rangle \\ &\quad + \langle\check{\mathcal{M}}(\phi^n)\nabla_h(-\varepsilon^2\Delta_h\tilde\phi^{n+1} + \sigma(-\Delta_h)^{-1}\tilde\phi^{n+1}), \nabla_h\tilde\phi^{n+1}\rangle,\end{aligned}$$

where $\mathcal{L}^{n+1}$ is defined as in Lemma 4.6. The lower bound for the $\mathcal{L}^{n+1}$ part is straightforward:

$$\begin{aligned}&\langle\check{\mathcal{M}}(\phi^n)\nabla_h\mathcal{L}^{n+1}, \nabla_h\tilde\phi^{n+1}\rangle \\ &\ge -\|\check{\mathcal{M}}(\phi^n)\|_\infty\cdot\|\nabla_h\mathcal{L}^{n+1}\|_2\cdot\|\nabla_h\tilde\phi^{n+1}\|_2 \\ &\ge -\mathcal{M}_1\|\nabla_h\mathcal{L}^{n+1}\|_2\cdot\|\nabla_h\tilde\phi^{n+1}\|_2 \ge -\frac{\mathcal{M}_1}{2}(\|\nabla_h\mathcal{L}^{n+1}\|_2^2 + \|\nabla_h\tilde\phi^{n+1}\|_2^2).\end{aligned} \tag{59}$$

An application of summation by parts implies that

$$-\langle\nabla_h\tilde\phi^{n+1}, \check{\mathcal{M}}(\phi^n)\nabla_h\Delta_h\tilde\phi^{n+1}\rangle = \langle\nabla_h\cdot(\check{\mathcal{M}}(\phi^n)\nabla_h\tilde\phi^{n+1}), \Delta_h\tilde\phi^{n+1}\rangle.$$

With a detailed finite difference expansion, we see that

$$\begin{aligned}\nabla_h \cdot (\check{\mathcal{M}}(\phi^n)\nabla_h\tilde{\phi}^{n+1})_{i,j,k} = \mathcal{M}(\phi^n)_{i,j,k}\Delta_h\tilde{\phi}^{n+1}_{i,j,k} + \frac{1}{2}\nabla_h\mathcal{M}(\phi^n)_{i,j,k}(\nabla_h\tilde{\phi}^{n+1}_{i,j,k})^\top \\ + \frac{1}{2}\nabla_h\mathcal{M}(\phi^n)_{i-1,j-1,k-1}(\nabla_h\tilde{\phi}^{n+1}_{i-1,j-1,k-1})^\top.\end{aligned}$$

This leads to the following estimate:

$$\begin{aligned}&-\langle\nabla_h\tilde{\phi}^{n+1}, \check{\mathcal{M}}(\phi^n)\nabla_h\Delta_h\tilde{\phi}^{n+1}\rangle \\ &\geq -\|\nabla_h\mathcal{M}(\phi^n)\|_4\cdot\|\nabla_h\tilde{\phi}^{n+1}\|_4\cdot\|\Delta_h\tilde{\phi}^{n+1}\|_2 + \mathcal{M}_0\|\Delta_h\tilde{\phi}^{n+1}\|_2^2,\end{aligned} \tag{60}$$

where the discrete Hölder inequality has been applied. Additionally, an application of the mean value theorem and the a-priori estimate (48) implies that

$$\|\nabla_h\mathcal{M}(\phi^n)\|_4 \leq \|\mathcal{M}'(\xi)\|_\infty\cdot\|\nabla_h\phi^n\|_4 \leq M\cdot\tilde{C}_3,$$

Referring back to (60), the following estimate becomes valid:

$$\begin{aligned}&-\langle\nabla_h\tilde{\phi}^{n+1}, \check{\mathcal{M}}(\phi^n)\nabla_h\Delta_h\tilde{\phi}^{n+1}\rangle \\ &\geq \mathcal{M}_0\|\Delta_h\tilde{\phi}^{n+1}\|_2^2 - M\tilde{C}_3\|\nabla_h\tilde{\phi}^{n+1}\|_4\cdot\|\Delta_h\tilde{\phi}^{n+1}\|_2 \\ &\geq \mathcal{M}_0\|\Delta_h\tilde{\phi}^{n+1}\|_2^2 - CM\tilde{C}_3\|\nabla_h\tilde{\phi}^{n+1}\|_2^{\frac{1}{4}}\cdot\|\Delta_h\tilde{\phi}^{n+1}\|_2^{\frac{3}{4}}\cdot\|\Delta_h\tilde{\phi}^{n+1}\|_2 \\ &\geq \mathcal{M}_0\|\Delta_h\tilde{\phi}^{n+1}\|_2^2 - CM\tilde{C}_3\|\nabla_h\tilde{\phi}^{n+1}\|_2^{\frac{1}{4}}\cdot\|\Delta_h\tilde{\phi}^{n+1}\|_2^{\frac{7}{4}} \\ &\geq \mathcal{M}_0\|\Delta_h\tilde{\phi}^{n+1}\|_2^2 - \frac{1}{2}\mathcal{M}_0\|\Delta_h\tilde{\phi}^{n+1}\|_2^2 - M^{(1)}\|\nabla_h\tilde{\phi}^{n+1}\|_2^2 \\ &= \frac{1}{2}\mathcal{M}_0\|\Delta_h\tilde{\phi}^{n+1}\|_2^2 - M^{(1)}\|\nabla_h\tilde{\phi}^{n+1}\|_2^2,\end{aligned} \tag{61}$$

in which the Sobolev inequality (see Lemma 2.4) is utilized in the second step, and the Young's inequality is employed in the final step. Moreover, $M^{(1)}$ depends only on $\mathcal{M}_0$, $\tilde{C}_3$ and $M$. Moreover, the following estimate for the nonlocal term could be derived with the help of Lemma 4.7:

$$\begin{aligned}&\sigma\langle\check{\mathcal{M}}(\phi^n)\nabla_h\tilde{\psi}^{n+1}, \nabla_h\tilde{\phi}^{n+1}\rangle \\ &\geq -\sigma\|\check{\mathcal{M}}(\phi^n)\|_\infty\cdot\|\nabla_h\tilde{\psi}^{n+1}\|_2\cdot\|\nabla_h\tilde{\phi}^{n+1}\|_2 \\ &\geq -\sigma\tilde{C}_4\mathcal{M}_1\|\tilde{\phi}^{n+1}\|_2\cdot\|\nabla_h\tilde{\phi}^{n+1}\|_2 \geq -\frac{\sigma^2\tilde{C}_4{}^2\mathcal{M}_1^2}{4}\|\tilde{\phi}^{n+1}\|_2^2 - \|\nabla_h\tilde{\phi}^{n+1}\|_2^2.\end{aligned} \tag{62}$$

The technique utilized in (51) could be similarly implemented to the first term on the right-hand side of (57)

$$\begin{aligned}&-2\langle(\check{\mathcal{M}}(\hat{\Phi}^n) - \check{\mathcal{M}}(\phi^n))\nabla_h\hat{\mu}^{n+1}, \nabla_h\tilde{\phi}^{n+1}\rangle \\ &\leq 2\|\nabla_h\hat{\mu}^{n+1}\|_\infty\cdot\|\check{\mathcal{M}}(\hat{\Phi}^n) - \check{\mathcal{M}}(\phi^n)\|_2\cdot\|\nabla_h\tilde{\phi}^{n+1}\|_2 \\ &\leq 2C^\star M\|\tilde{\phi}^n\|_2\cdot\|\nabla_h\tilde{\phi}^{n+1}\|_2 \leq (C^\star)^2M^2\|\tilde{\phi}^n\|_2^2 + \|\nabla_h\tilde{\phi}^{n+1}\|_2^2.\end{aligned} \tag{63}$$

Substituting (58) - (63) into (57) and applying Lemma 4.6, we obtain

$$\begin{aligned}
&\frac{1}{\Delta t}\left(\|\tilde{\phi}^{n+1}\|_2^2-\|\tilde{\phi}^{n}\|_2^2\right)+\varepsilon^2\mathcal{M}_0\|\Delta_h\tilde{\phi}^{n+1}\|_2^2\\
&\le\left(48\mathcal{M}_1(\varepsilon_0^\star)^{-2}+\mathcal{M}_1+2\varepsilon^2M^{(1)}+3\right)\|\nabla_h\tilde{\phi}^{n+1}\|_2^2+3\mathcal{M}_1\theta_0^2\|\nabla_h\tilde{\phi}^{n}\|_2^2\\
&\quad+\frac{\sigma^2\mathcal{M}_1^2\tilde{C}_4{}^2}{2}\|\tilde{\phi}^{n+1}\|_2^2+(C^\star)^2M^2\|\tilde{\phi}^{n}\|_2^2+\|\tau^{n+1}\|_2^2+3C\mathcal{M}_1(\varepsilon_0^\star)^{-4}\|\tilde{\phi}^{n+1}\|_4^2\\
&\le M^{(2)}\|\nabla_h\tilde{\phi}^{n+1}\|_2^2+M^{(3)}\|\nabla_h\tilde{\phi}^{n}\|_2^2+M^{(4)}\|\tilde{\phi}^{n+1}\|_2^2+M^{(5)}\|\tilde{\phi}^{n}\|_2^2+\|\tau^{n+1}\|_2^2,
\end{aligned}\tag{64}$$

with the constant representations

$$\begin{aligned}
&M^{(2)}=48\mathcal{M}_1(\varepsilon_0^\star)^{-2}+3C\mathcal{M}_1(\varepsilon_0^\star)^{-4}+\mathcal{M}_1+2\varepsilon^2M^{(1)}+3,\\
&M^{(3)}=3\mathcal{M}_1\theta_0^2,\qquad M^{(4)}=\frac{\sigma^2\mathcal{M}_1^2\tilde{C}_4{}^2}{2},\qquad M^{(5)}=(C^\star)^2M^2.
\end{aligned}$$

In the derivation, the 3D discrete Sobolev inequality and the bound $\|\cdot\|_4\le C\|\cdot\|_{H_h^1}$ have been utilized. Meanwhile, an application of Cauchy inequality indicates that

$$\begin{aligned}
M^{(2)}\|\nabla_h\tilde{\phi}^{n+1}\|_2^2&\le\frac{\varepsilon^2\mathcal{M}_0}{4}\|\Delta_h\tilde{\phi}^{n+1}\|_2^2+\frac{(M^{(2)})^2}{\varepsilon^2\mathcal{M}_0}\|\tilde{\phi}^{n+1}\|_2^2,\\
M^{(3)}\|\nabla_h\tilde{\phi}^{n}\|_2^2&\le\frac{\varepsilon^2\mathcal{M}_0}{4}\|\Delta_h\tilde{\phi}^{n}\|_2^2+\frac{(M^{(3)})^2}{\varepsilon^2\mathcal{M}_0}\|\tilde{\phi}^{n}\|_2^2.
\end{aligned}$$

Subsequently, inequality (64) can be transformed into the following form

$$\begin{aligned}
&\frac{1}{\Delta t}(\|\tilde{\phi}^{n+1}\|_2^2-\|\tilde{\phi}^{n}\|_2^2)+\frac{3}{4}\varepsilon^2\mathcal{M}_0\|\Delta_h\tilde{\phi}^{n+1}\|_2^2-\frac{1}{4}\varepsilon^2\mathcal{M}_0\|\Delta_h\tilde{\phi}^{n}\|_2^2\\
&\le\Big(\frac{(M^{(2)})^2}{\varepsilon^2\mathcal{M}_0}+M^{(4)}+1\Big)\|\tilde{\phi}^{n+1}\|_2^2+\Big(\frac{(M^{(3)})^2}{\varepsilon^2\mathcal{M}_0}+M^{(5)}\Big)\|\tilde{\phi}^{n}\|_2^2+\|\tau^{n+1}\|_2^2.
\end{aligned}$$

Therefore, with sufficiently small $\Delta t$ and $h$, an application of discrete Gronwall inequality results in the desired higher-order convergence estimate

$$\|\tilde{\phi}^{n+1}\|_2+\Big(\varepsilon^2\mathcal{M}_0\Delta t\sum_{k=1}^{n+1}\|\Delta_h\tilde{\phi}^{k}\|_2^2\Big)^{1/2}\le C(\Delta t^2+h^2),\tag{65}$$

based on the truncation error accuracy, $\|\tau^{n+1}\|_2\le C(\Delta t^2+h^2)$. This finishes the refined error estimate.

Moreover, it is necessary to recover the a-priori assumption (45) at the next time step $t_{n+1}$ to enable the analysis to proceed in an inductive manner. Under the linear refinement constraint $C_1h\le\Delta t\le C_2h$, the convergence estimate (65) indicates that

$$\begin{aligned}
&\|\tilde{\phi}^{n+1}\|_2\le C(\Delta t^2+h^2)\le\Delta t^{\frac{15}{8}}+h^{\frac{15}{8}},\\
&\|\Delta_h\tilde{\phi}^{n+1}\|_2\le\frac{C(\Delta t^2+h^2)}{\Delta t^{\frac12}}\le C(\Delta t^{\frac32}+h^{\frac32})\le\Delta t^{\frac{11}{8}}+h^{\frac{11}{8}},
\end{aligned}$$

provided that $\Delta t$ and $h$ are sufficiently small.

The error estimate (24) for the variable $\phi$ follows directly from (65), in conjunction with the bound of the supplementary fields $\Phi_{\Delta t}$ and the projection approximation (22). This completes the proof of Theorem 4.1.

**Remark 4.8.** The proposed numerical scheme (5) is only first order accurate in time. In the future works, an extension to the second order schemes will be considered. The primary challenge is associated with the second order accurate approximation to the nonlinear and singular logarithmic term while preserving an energy stability, combined with the second order and numerically stable approximation to the mobility function and the nonlocal term. In terms of the convergence analysis for the second order scheme, higher-order temporal and spatial correction functions will be necessary to facilitate a smooth analysis process. In addition, more advanced techniques, different from those used in the first order scheme, may be required.

## 5. Numerical experiments.

Due to the tendency to minimize the area of interface, the morphology of final patterns in phase transitions usually decomposes into simple subdomains after the coarsening process. However, if there is a microscopic constraint on the system, the final pattern becomes much richer. Experimentally, the final equilibrium state often prefers periodic structures such as lamellar, labyrinthine, columnar, spherical, double-diamond geometries and other more complex structures (see, for example, [2, 3, 33, 34, 37]). In this section, we present a few numerical results, including some experiments designed to verify relevant properties and convergence tests. The theoretical analysis is valid for both 2D and 3D situations; however, we choose the 2D domain for simplicity. A nonlinear full approximation storage (FAS) multigrid solver is used to solve the convex-concave decomposition scheme for the NCH equation with logarithmic potential. See [11, 13] for the related details of a similar solver. We compare the numerical results with some references [15, 16] to confirm the validity of the numerical scheme.

### 5.1. Asymptotic convergence test.

We first present a convergence test for the numerical scheme. The smooth initial condition is taken to be

$$\phi(x, y, 0) = 0.25 \cos 2\pi x \cos 2\pi y + 0.6 \cos \pi x \cos 3\pi y. \tag{66}$$

The mobility is selected as $\mathcal{M}(\phi) = 0.9(1-\phi)(1+\phi) + 0.1$. To determine the convergence rate, the error function is computed between approximate solutions obtained by successively finer mesh sizes. The parameters are set as: $L = L_x = L_y = 2$, $\varepsilon = 0.2$, $\theta_0 = 3.0$, $\sigma = 1 \times 10^{-3}$, $T = 1$.We expect the scheme to have an accuracy of order $O(\Delta t + h^2)$. The refinement path is set as $\Delta t = 0.02h^2$, which naturally implies first-order temporal convergence when second-order spatial convergence is achieved. The results of the numerical convergence test, presented in Table 1, confirm second-order accuracy in space and first-order accuracy in time.

TABLE 1. Numerical convergence test with initial data (66) at $T = 1$

| Grid size | $16^2 - 32^2$ | $32^2 - 64^2$ | $64^2 - 128^2$ | $128^2 - 256^2$ |
|---|---|---|---|---|
| $L^2$ error | 4.8490E-03 | 1.3554E-03 | 3.3769E-04 | 8.3877E-05 |
| $L^2$ rate | — | 1.8390 | 2.0049 | 2.0093 |
| $L^\infty$ error | 9.3305E-03 | 2.6855E-03 | 6.7400E-04 | 1.6793E-04 |
| $L^\infty$ rate | — | 1.7968 | 1.9944 | 2.0049 |

5.2. **Algebraic convergence tests for the multigrid solver.** To demonstrate that our FAS multigrid solver achieves optimal or near-optimal complexity for the proposed numerical scheme, we conducted a series of algebraic convergence tests. The setup follows that of the previous subsection, except a fixed time step size $\Delta t = 0.01$ is used for all simulations in this test. The multigrid stopping tolerance is taken to be $\tau = 10^{-10}$. We plot the residual $\|r^n\|_2$ against the multigrid iteration count $n$ on a semi-logarithmic scale at $T = 0.1$. The results, shown in Figure 1, indicate that the residual decreases by an almost constant factor per iteration, clearly demonstrating the solver's high efficiency.

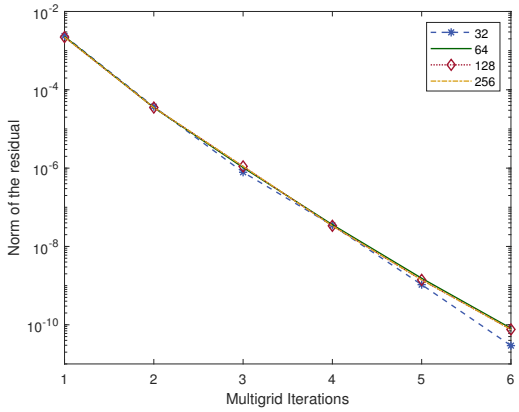


FIGURE 1. Convergence test of the FAS multigrid solver for the numerical scheme (5), with grid sizes set to 32, 64, 128, and 256, respectively.

5.3. **Spinodal decomposition.** The phase separation process can be studied by considering a homogeneous binary mixture. In this case, the system undergoes spinodal decomposition, transitioning from a homogeneous state to a two-phase state [5, 19]. In this subsection, we choose random initial data to simulate a homogeneous binary mixture and present the phase decomposition phenomenon, energy decay as well as mass conservation by varying the parameters.

5.3.1. *The phase separation.* We first select a very small nonlocal parameter, $\sigma = 0.001$. With this choice, the NCH model is expected to be consistent with the standard CH model. We set $\Omega = [0, 2\pi]^2$ and take parameters as $\varepsilon = 0.06$, $\theta_0 = 3.0$, $h = 1/256$, $\Delta t = 1.0 \times 10^{-3}$. The mobility and the initial conditions are chosen to be

$$\mathcal{M}(\phi) = 0.9(1-\phi)(1+\phi) + 0.1, \quad \phi^0_{i,j} = \overline{\phi^0} + 0.01\, r_{i,j}, \tag{67}$$

where $r_{i,j}$ is a uniformly distributed random variable in $[-1, 1]$ with zero mean.

Take the initial value as $\overline{\phi^0} = 0$, which indicates that the volumes of two components are nearly identical. As depicted in Figure 2, phase separation occurs at the very beginning, leading to the formation of lamellar nanostructures by around $t = 200$. Subsequently, we modify the parameters to $\overline{\phi^0} = 0.3$, signifying that the volume of the red region exceeds that of the blue region. The evolution of the phase variable at selected time instants is presented in Figure 3. As can be seen, the

dynamics differs significantly from the case where $\overline{\phi^0} = 0$. During this process, the region with the less volume merges and eventually accumulates into a circular pattern. These results, simulated by the numerical scheme (5), are consistent with the experimental observations of lamellar phases and spherical states [3]. It is also observed that the coarsening dynamics requires more time to reach a near-stationary state, in comparison with the constant mobility cases reported in [13], due to the reduced bulk diffusion.

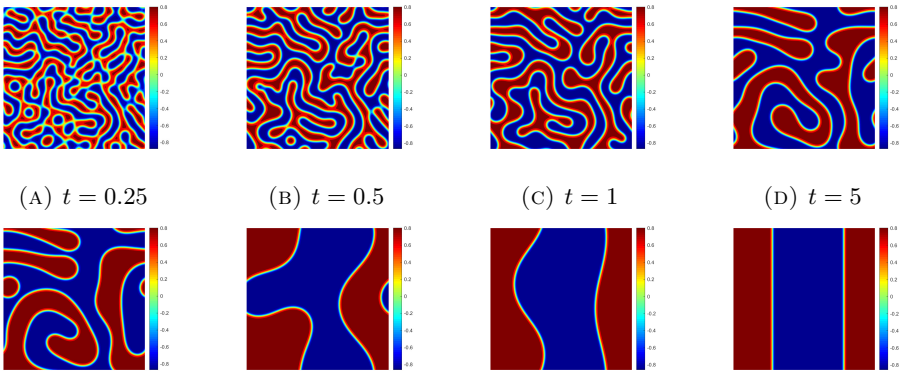

(A) $t = 0.25$ (B) $t = 0.5$ (C) $t = 1$ (D) $t = 5$

(E) $t = 10$ (F) $t = 100$ (G) $t = 200$ (H) $t = 800$

FIGURE 2. Evolution of the phase variable for $\sigma = 0.001$ at selected time instants, with the mobility and initial condition described in (67), where $\overline{\phi^0} = 0$.

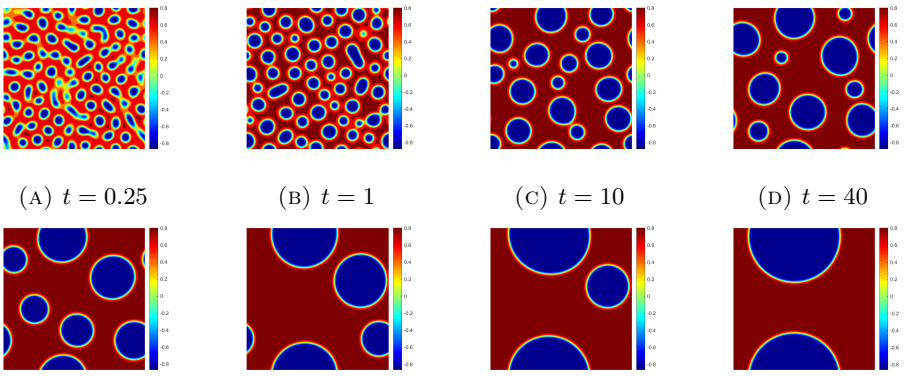

(A) $t = 0.25$ (B) $t = 1$ (C) $t = 10$ (D) $t = 40$

(E) $t = 100$ (F) $t = 200$ (G) $t = 400$ (H) $t = 800$

FIGURE 3. Evolution of the phase variable for $\sigma = 0.001$ at selected time instants, with the mobility and initial condition described in (67), where $\overline{\phi^0} = 0.3$.

5.3.2. *The nonlocal parameter.* Now we investigate the interface shapes governed by the NCH equation (3) with different nonlocal parameters $\sigma$. The mobility and

the initial conditions are also set as the ones specified in (67). We begin with increasing the nonlocal parameter to $\sigma = 5$ while keeping the initial value $\overline{\phi^0} = 0$. The mobility and other parameters are consistent with those used in the previous section. Figure 4 reveals that the initial phase separation dynamics resembles those observed for $\sigma = 0.001$ with $\overline{\phi^0} = 0$, as shown in Figure 2. However, the final lamellar pattern differs significantly, and equilibrium state is reached at $t = 100$, which occurs much more rapidly compared to the case with $\sigma = 0.001$ and $\overline{\phi^0} = 0$.

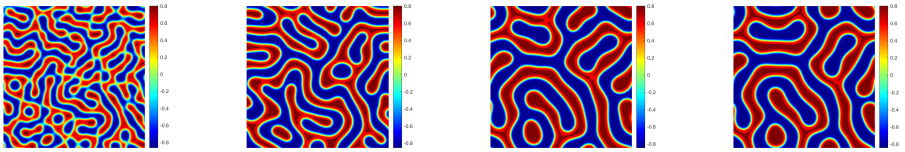

(A) $t = 0.25$ (B) $t = 1$ (C) $t = 100$ (D) $t = 600$

FIGURE 4. Evolution of the phase variable for $\sigma = 5$ at selected time instants, with the mobility and initial condition described in (67), where $\overline{\phi^0} = 0$.

Figure 5 displays the results for a nonlocal parameter $\sigma = 10$ with an initial value $\overline{\phi^0} = 0.3$. The preliminary stage of phase separation is also consistent with the case of $\sigma = 0.001$, $\overline{\phi^0} = 0.3$, as depicted in Figure 3. However, the final steady state exhibits a circular pattern with a significantly smaller radius.

The nonlocal parameter $\sigma$ represents long-range interactions (e.g., microphase separation of block copolymers). Large $\sigma$ accelerates the dynamics of phase separation but suppresses coarsening, aligning with Ohta-Kawasaki theory [48], indicating that the nonlocal term stabilizes periodic microstructures rather than the macroscopic one. As observed in experiments [3, 37], the equilibrium states under nonlocal effects exhibit rich periodic patterns (e.g., lamellar, labyrinthine, columnar, and spherical geometries). Our numerical results (Figures. 2–5) further validate this: increasing $\sigma$ from 0.001 to 10 shifts the final steady state from the macroscopic domains (Figures. 2–3) to microphase separated structures (Figures. 4–5). Specifically, lamellar patterns stabilize rapidly at $\sigma = 5$ (Figure 4), while smaller spherical domains dominate at $\sigma = 10$ (Figure 5), consistent with the theoretical expectation.

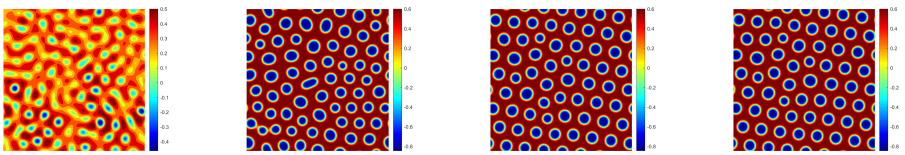

(A) $t = 0.25$ (B) $t = 2$ (C) $t = 60$ (D) $t = 100$

FIGURE 5. Evolution of the phase variable for $\sigma = 10$ at selected time instants, with the mobility and initial condition described in (67), where $\overline{\phi^0} = 0.3$.

5.3.3. *The variable mobility.* In the initial numerical experiment, $\mathcal{M}(\phi)$ was set to (67), based on references [9, 10, 52, 57]. This choice was discussed in the introduction section, particularly in connection with equation (4). Meanwhile, it is observed that, when the numerical solutions rapidly achieved phase separation and entered the coarsening stage (where $\phi$ approaches $\pm 1$), (67) led to nearly identical mobility within each component. To avoid this limitation, we introduce an alternative mobility form,

$$\mathcal{M}(\phi) = \frac{1}{4}\phi + \frac{1}{2}. \tag{68}$$

This form not only satisfies the requirements for $\mathcal{M}(\phi)$ in Theorems 3.3, 3.4, and 4.1, but also ensures distinct values for mobility within each component during the coarsening stage. The initial condition and other parameters are kept the same as in the case with $\overline{\phi^0} = 0$ in section 5.3.1. Figure 6 displays the evolution of $\phi$ at various time instants up to $T = 800$. Interestingly, a circular interface emerges, in contrast with the lamellar structure observed in Figure 2.

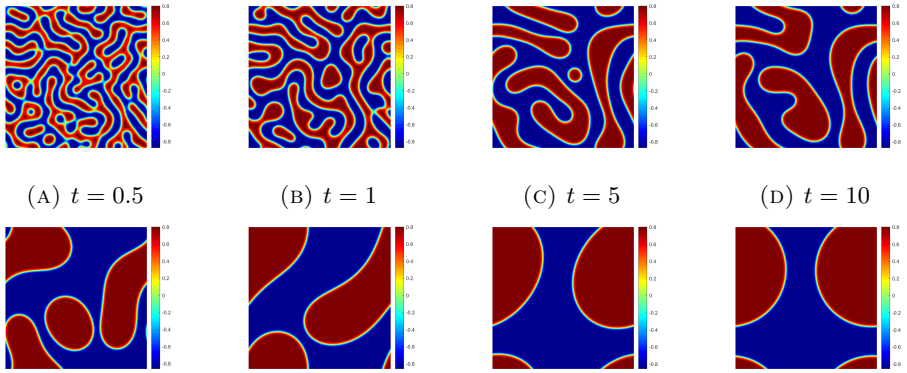

(A) $t = 0.5$ (B) $t = 1$ (C) $t = 5$ (D) $t = 10$

(E) $t = 50$ (F) $t = 100$ (G) $t = 400$ (H) $t = 800$

FIGURE 6. Evolution of the phase variable for the mobility given by (68).

5.4. **Positivity preserving, energy decay and mass conservation.** In this section, we verify some mathematical properties of the numerical scheme, including positivity preservation, energy decay, and mass conservation. We calculate the maximum and minimum values of the phase variable, which are presented in Table 2. Figures 2 and 3, along with Table 2 and Figure 7, clearly indicate notable distances between the extrema of the phase variable and the singular limit values $\pm 1$, confirming the phase separation property. These numerical results provide strong evidence that the numerical scheme preserves the positivity of the singular logarithmic energy potential.

There have been many existing numerical works to deal with CH equation with Flory-Huggins style energy potential, either with or without nonlocal diffusion part. For many numerical approaches using an explicit approximation to the logarithmic terms (e.g., [50]), the positivity of the logarithmic arguments could not be theoretically justified, which comes from the explicit computation of the logarithmic terms. In turn, an extended definition of the Flory-Huggins style energy has to be

TABLE 2. Maximum and minimum values of $\phi$ during spinodal decomposition

| | $\overline{\phi^0} = 0$, $\sigma = 0.001$ | | $\overline{\phi^0} = 0.3$, $\sigma = 0.001$ | |
|---|---|---|---|---|
| t | minimum | maximum | minimum | maximum |
| 0 | -0.0099994 | 0.0099993 | 0.2900006 | 0.3099993 |
| 0.25 | -0.8771207 | 0.8738842 | -0.8679642 | 0.8172793 |
| 0.50 | -0.8699566 | 0.8749814 | -0.8780085 | 0.8473611 |
| 1 | -0.8714909 | 0.8726312 | -0.8781753 | 0.8474252 |
| 5 | -0.8708642 | 0.8705946 | -0.8783427 | 0.8519701 |
| 10 | -0.8703183 | 0.8713044 | -0.8784810 | 0.8482916 |
| 100 | -0.8650477 | 0.8645630 | -0.86886334 | 0.8524863 |
| 800 | -0.8584575 | 0.8584574 | -0.8614907 | 0.8553786 |

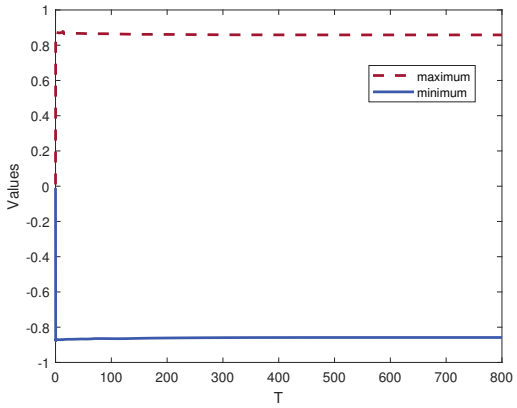


FIGURE 7. The maximum and minimum values over time, where $\overline{\phi^0} = 0$, $\sigma = 0.001$.

introduced to establish the associated energy estimate, since the energy has to be redefined if the phase variable stays beyond the positivity requirement. In comparison, the proposed numerical scheme in this work preserves the positivity of the logarithmic arguments, namely $1 - \phi$ and $1 + \phi$, at a theoretical level. As a result, there is no need to post-processing for the phase variable, since the positivity-preserving property has been theoretically guaranteed. This fact demonstrates a clear advantage of the proposed numerical scheme over many classical numerical methods.

Energy and mass evolutions for the aforementioned cases are depicted in Figure 8, where mob1 $= 0.9(1 - \phi)(1 + \phi) + 0.1$ and mob2 $= \frac{1}{4}\phi + \frac{1}{2}$. These curves illustrate that the numerical algorithm is unconditionally energy stable and mass conservative.

6. **Conclusions.** In this paper, we investigate a positivity-preserving, energy stable finite difference scheme for the variable mobility nonlocal CH system with a logarithmic Flory-Huggins energy potential. To ensure the positivity-preserving property, the convex splitting method is applied. This involves treating the nonlinear logarithmic terms, the surface diffusion term, and the nonlocal term implicitly,

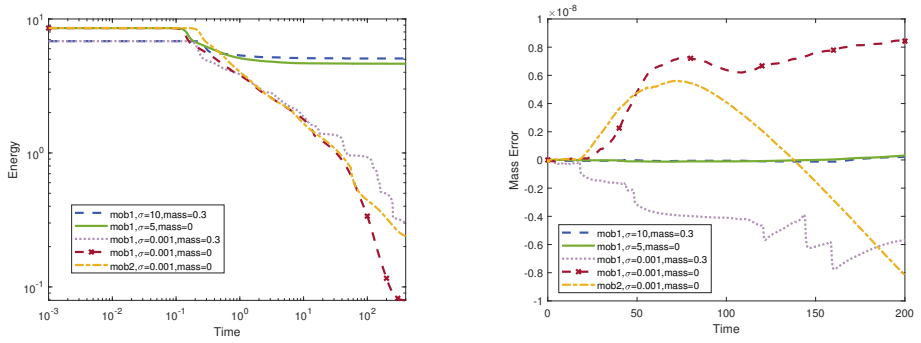


(A) Energy (B) Mass Error

FIGURE 8. Energy decay and mass conservation for five cases, where the mobility is chosen as either mob1 $= 0.9(1-\phi)(1+\phi)+0.1$ or mob2 $= \phi/4 + 1/2$, depending on the case.

combined with an explicit update of the expansive concave term and the mobility. Such a numerical approach also guarantees an unconditional energy stability. Furthermore, an optimal convergence rate analysis and error estimate have been theoretically derived through higher-order consistency analysis, in conjunction with rough and refined error estimates. Several numerical experiments are conducted with the nonlocal term parameterized by $\sigma$ to confirm the consistency between NCH model and standard CH model, to investigate the phase separation phenomenon with different choices of initial condition and $\sigma$, and to verify the optimal convergence rates in both temporal and spatial discretizations.

**Acknowledgments.** C. Wang is partially supported by the NSF DMS-2012269, DMS-2309548, and Z.R. Zhang is partially supported by the NSFC No.11871105 and 12231003.

## REFERENCES

[1] A. Aristotelous, O. Karakashian and S. M. Wise, A mixed discontinuous galerkin, convex splitting scheme for a modified Cahn-Hilliard equation and an efficient nonlinear multigrid solver, *Discrete Contin. Dyn. Syst. Ser. B*, **18** (2013), 2211-2238.

[2] M. Bahiana and Y. Oono, Cell dynamical system approach to block copolymers, *Phys. Rev. A*, **41** (1990), 6763.

[3] F. S. Bates and G. H. Fredrickson, Block copolymers-designer soft materials, *Phys. today*, **52** (1999), 32–38.

[4] A. L. Bertozzi, S. Esedoglu and A. Gillette, Inpainting of binary images using the Cahn-Hilliard equation, *IEEE Trans. Image Process.*, **16** (2006), 285-291.

[5] K. Binder, Collective diffusion, nucleation, and spinodal decomposition in polymer mixtures, *J. Chem. Phys.*, **79** (1983), 6387-6409.

[6] R. B. Bird, R. C. Armstrong and O. Hassager, Dynamics of polymeric liquids, *J. Fluid Mech.*, **1** (1987).

[7] J. W. Cahn, C. M. Elliott and A. Novick-Cohen, The Cahn-Hilliard equation with a concentration dependent mobility: Motion by minus the laplacian of the mean curvature, *Eur. J. Appl. Math.*, **7** (1996), 287-301.

[8] J. W. Cahn and J. E. Hilliard, Free energy of a nonuniform system. I. interfacial free energy, *J. Chem. Phys.*, **28** (1958), 258-267.

[9] J. W. Cahn and J. E. Hilliard, Spinodal decomposition: A reprise, *Acta Metall.*, **19** (1971), 151-161.

[10] J. W. Cahn and J. E. Taylor, Surface motion by surface diffusion, *Acta Metall. Mater.*, **42** (1994), 1045-1063.
[11] L. Chen, X. Hu and S. M. Wise, Convergence analysis of the fast subspace descent method for convex optimization problems, *Math. Comput.*, **89** (2020), 2249-2282.
[12] W. Chen, J. Jing, C. Wang, X. Wang and S. M. Wise, A modified Crank-Nicolson scheme for the Flory-Huggins Cahn-Hilliard model, *Commun. Comput. Phys.*, **31** (2022), 60-93.
[13] W. Chen, C. Wang, X. Wang and S. M. Wise, Positivity-preserving, energy stable numerical schemes for the Cahn-Hilliard equation with logarithmic potential, *J. Comput. Phys.*, **3** (2019), 100031.
[14] X. C. Chen, C. Wang and S. M. Wise, A preconditioned steepest descent solver for the Cahn-Hilliard equation with variable mobility, *Int. J. Numer. Anal. Model*, **19** (2022), 839-863.
[15] Q. Cheng, X. Yang and J. Shen, Efficient and accurate numerical schemes for a hydrodynamically coupled phase field diblock copolymer model, *J. Comput. Phys.*, **341** (2017), 44-60.
[16] R. Choksi, M. Maras and J. F. Williams, 2D phase diagram for minimizers of a Cahn-Hilliard functional with long-range interactions, *SIAM J. Appl. Dyn. Syst.*, **10** (2011), 1344-1362.
[17] R. Choksi, M. A. Peletier and J. F. Williams, On the phase diagram for microphase separation of diblock copolymers: An approach via a nonlocal Cahn-Hilliard functional, *SIAM J. Appl. Math.*, **69** (2009), 1712-1738.
[18] M. I. M. Copetti and C. M. Elliott, Numerical analysis of the Cahn-Hilliard equation with a logarithmic free energy, *Numer. Math.*, **63** (1992), 39-65.
[19] P. G. De Gennes, Dynamics of fluctuations and spinodal decomposition in polymer blends, *J. Chem. Phys.*, **72** (1980), 4756-4763.
[20] M. Doi, *Soft Matter Physics*, Oxford University Press, Oxford, 2013.
[21] M. Doi and S. F. Edwards, *The Theory of Polymer Dynamics*, Oxford University Press, 1988.
[22] L. Dong, W. Feng, C. Wang, S. M. Wise and Z. Zhang, Convergence analysis and numerical implementation of a second order numerical scheme for the three-dimensional phase field crystal equation, *Comput. Math. Appl.*, **75** (2018), 1912-1928.
[23] Q. Du, L. Ju, X. Li and Z. Qiao, Stabilized linear semi-implicit schemes for the nonlocal Cahn-Hilliard equation, *J. Comput. Phys.*, **363** (2018), 39-54.
[24] C. M. Elliott and H. Garcke, On the Cahn-Hilliard equation with degenerate mobility, *SIAM J. Math. Anal.*, **27** (1996), 404-423.
[25] D. J. Eyre, Unconditionally gradient stable time marching the Cahn-Hilliard equation, *Mater. Res. Soc. Symp. Proc.*, **529** (1998), 39-46.
[26] P. C. Fife, Some nonclassical trends in parabolic and parabolic-like evolutions, *Trends in Nonlinear Analysis*, Springer, Berlin, (2003), 153-191.
[27] C. G. Gal, A. Giorgini and M. Grasselli, The separation property for 2D Cahn-Hilliard equations: Local, nonlocal and fractional energy cases, *Discrete Contin. Dyn. Syst.*, **43** (2023), 2270-2304.
[28] Z. Guan, J. S. Lowengrub and C. Wang, Convergence analysis for second-order accurate schemes for the periodic nonlocal Allen-Cahn and Cahn-Hilliard equations, *Math. Methods Appl. Sci.*, **40** (2017), 6836-6863.
[29] Z. Guan, J. S. Lowengrub, C. Wang and S. M. Wise, Second order convex splitting schemes for periodic nonlocal Cahn-Hilliard and Allen-Cahn equations, *J. Comput. Phys.*, **277** (2014), 48-71.
[30] Z. Guan, C. Wang and S. M. Wise, A convergent convex splitting scheme for the periodic nonlocal Cahn-Hilliard equation, *Numer. Math.*, **128** (2014), 377-406.
[31] Y. Guo, C. Wang, S. Wise and Z. Zhang, Convergence analysis of a positivity-preserving numerical scheme for the Cahn-Hilliard-Stokes system with Flory-Huggins energy potential, *Math. Comput.*, **93** (2024), 2185-2214.
[32] I. W. Hamley, *The Physics of Block Copolymers*, Oxford University Press, Oxford, 1998.
[33] H. Hasegawa, H. Tanaka, K. Yamasaki and T. Hashimoto, Bicontinuous microdomain morphology of block copolymers. 1. Tetrapod-network structure of polystyrene-polyisoprene diblock polymers, *Macromolecules*, **20** (1987), 1651-1662.
[34] T. Hashimoto, M. Shibayama and H. Kawai, Ordered structure in block polymer solutions. 4. Scaling rules on size of fluctuations with block molecular weight, concentration, and temperature in segregation and homogeneous regimes, *Macromolecules*, **16** (1983), 1093-1101.

[35] M. Henry and Y. Nishiura, Singular limit of a second order nonlocal parabolic equation of conservative type arising in the micro-phase separation of diblock copolymers, *Hokkaido Math. J.*, **32** (2003), 561-622.
[36] D. Jeong, J. Shin, Y. Li, Y. Choi, J. H. Jung, S. Lee and J. Kim, Numerical analysis of energy-minimizing wavelengths of equilibrium states for diblock copolymers, *Curr. Appl. Phys.*, **14** (2014), 1263-1272.
[37] A. K. Khandpur, S. Foerster, F. S. Bates, et al., Polyisoprene-polystyrene diblock copolymer phase diagram near the order-disorder transition, *Macromolecules*, **28** (1995), 8796-8806.
[38] X. Li, Z. Qiao and C. Wang, Convergence analysis for a stabilized linear semi-implicit numerical scheme for the nonlocal Cahn-Hilliard equation, *Math. Comp.*, **90** (2021), 171-188.
[39] X. Li, Z. Qiao and C. Wang, Stabilization parameter analysis of a second order linear numerical scheme for the nonlocal Cahn-Hilliard equation, *IMA J. Numer. Anal.*, **43** (2023), 1089-1114.
[40] X. Li, Z. Qiao and C. Wang, Double stabilizations and convergence analysis of a second-order linear numerical scheme for the nonlocal Cahn-Hilliard equation, *Sci. China Math.*, **67** (2024), 187-210.
[41] Y. Li, Q. Xia, C. Lee, S. Kim and J. Kim, A robust and efficient fingerprint image restoration method based on a phase-field model, *Pattern Recogn.*, **123** (2022), 108405.
[42] R. C. Merton, Option pricing when underlying stock returns are discontinuous, *J. Financ. Econ.*, **3** (1976), 125-144.
[43] C. B. Muratov, Theory of domain patterns in systems with long-range interactions of coulomb type, *Phys. Rev. E*, **66** (2002), 066108.
[44] Y. Nishiura, Mesoscopic morphology and scaling law of stationary interfacial patterns for reaction diffusion systems, *Equadiff 8*, **4** (1994), 169-173.
[45] Y. Nishiura and I. Ohnishi, Some mathematical aspects of the micro-phase separation in diblock copolymers, *Physica D*, **84** (1995), 31-39.
[46] I. Ohnishi and Y. Nishiura, Spectral comparison between the second and the fourth order equations of conservative type with nonlocal terms, *Jpn. J. Ind. Appl. Math.*, **15** (1998), 253-262.
[47] I. Ohnishi, Y. Nishiura, M. Imai and Y. Matsushita, Analytical solutions describing the phase separation driven by a free energy functional containing a long-range interaction term, *Chaos*, **9** (1999), 329-341.
[48] T. Ohta and K. Kawasaki, Equilibrium morphology of block copolymer melts, *Macromolecules*, **19** (1986), 2621-2632.
[49] L. M. Pismen, Nonlocal diffuse interface theory of thin films and the moving contact line, *Phys. Rev. E*, **64** (2001), 021603.
[50] Y. Qin, Z. Xu, H. Zhang and Z. Zhang, Fully decoupled, linear and unconditionally energy stable schemes for the binary fluid-surfactant model, *Commun. Comput. Phys.*, **28** (2020), 1389-1414.
[51] C. Sagui and R. C. Desai, Kinetics of phase separation in two-dimensional systems with competing interactions, *Phys. Rev. E*, **49** (1994), 2225.
[52] J. E. Taylor and J. W. Cahn, Linking anisotropic sharp and diffuse surface motion laws via gradient flows, *J. Stat. Phys.*, **77** (1994), 183-197.
[53] J. D. Van der Waals, The thermodynamic theory of capillarity under the hypothesis of a continuous variation of density, *J. Stat. Phys.*, **20** (1979), 200-244.
[54] C. Wang and S. M. Wise, An energy stable and convergent finite-difference scheme for the modified phase field crystal equation, *SIAM J. Numer. Anal.*, **49** (2011), 945-969.
[55] S. M. Wise, C. Wang and J. Lowengrub, An energy-stable and convergent finite-difference scheme for the phase field crystal equation, *SIAM J. Numer. Anal.*, **47** (2009), 2269-2288.
[56] X. F. Wu and Y. A. Dzenis, Phase-field modeling of the formation of lamellar nanostructures in diblock copolymer thin films under inplanar electric fields, *Phys. Rev. E*, **77** (2008), 031807.
[57] T. Zhang and Q. Wang, Cahn-Hilliard vs singular Cahn-Hilliard equations in phase field modeling, *Commun. Comput. Phys.*, **7** (2010), 362.

Received November 2024; 1st revision March 2025; 2nd revision June 2025; early access July 2025.